An Exploratory Analysis of Trends in Swordfish (*Xiphias gladius*) Length Composition Data from the Hawaiian Longline Fishery[1][2]

Michelle Sculley[a], Jon Brodziak[b], Annie Yau[b], Maia Kapur[a]

[a] Joint Institute for Marine and Atmospheric Research, University of Hawaii, c/o NOAA Fisheries, 1845 Wasp Blvd., Honolulu, HI, 96818

[b] NOAA Fisheries, National Marine Fisheries Service, Pacific Islands Fisheries Science Center, 1845 Wasp Blvd., Honolulu, HI, 96818

Abstract

Generalized additive models (GAMs) were applied to explore the relative influence of spatial, temporal, and environmental predictors on the distribution of swordfish (*Xiphias gladius*) fishery length frequency data from the Pacific Islands Regional Observer Program database on the Hawaiian longline fishery during 1994–2016. Spatial predictors were more generally influential on swordfish length than temporal factors. Environmental variables such as sea surface temperature, the Pacific Decadal Oscillation index, and the Southern Oscillation Index were sometimes significant but did not explain a substantial portion of the variance in the data. Models of the deep-set sector explained 30–50% of the deviance while models of the shallow-set sector explained less than 25% of the deviance. The deep-set sector does not target swordfish, primarily captures small young-of-the-year (<100cm) individuals, and had much higher annual variability in length. The shallow-set sector targets swordfish, catches primarily large swordfish, and has had relatively low annual variability. Spatial patterns indicate that large fish are caught in the more northern latitudes while smaller fish are caught closer to the equator. Overall, based on the significant differences between the length composition of the shallow-set and deep-set catch, the deep-set data is unlikely to be representative of the targeted swordfish fishery. However, the deep-set data did primarily consist of small fish with a median length of 82 cm and may contain information on annual recruitment strength. It would be useful to compare the patterns observed in this analysis with those from other fisheries to see if the conclusions drawn here are applicable to the entire North Pacific swordfish population.

[1] PIFSC Working Paper WP-17-002. Issued 21 June 2017. https://doi.org/10.7289/V5/WP-PIFSC-17-002.

[2] [1]Working document submitted to Intersessional Meeting of the Billfish Working Group, International Scientific Committee for Tuna and Tuna-like Species in the North Pacific Ocean, June 1-7, 2017, Keelung, Taiwan. Document not to be cited without author's permission.

Introduction

Broadbill swordfish (*Xiphias gladius*) inhabit the Pacific Ocean between 50°N and 50°S. They are a commercially important highly migratory species caught primarily by the Japanese, Taiwanese, and US longline fishery (Bigelow *et al.*, 1999). The swordfish in the North Pacific have been assessed as a single-stock scenario and under a two-stock scenario, with one stock in the western central Pacific Ocean and one stock in the eastern Pacific Ocean. These stocks were assessed in 2009 and again in 2014 by the Billfish Working Group of the International Scientific Committee for Tuna and Tuna-like Species in the North Pacific Ocean (ISC). The eastern Pacific Stock was also assessed by the Inter-American Tropical Tuna Commission (IATTC) in 2010.

The 2009 ISC stock assessment of swordfish in the North Pacific explored the use of length frequency data in Stock Synthesis 3 (SS3) models for both the single-stock and two-stock scenario. In the two-stock scenario, length frequency data were only included for the western and central stock in a preliminary age-structured assessment model. Ultimately, length frequency data were not used in the assessment of the western and central North Pacific and eastern Pacific stocks, and management recommendations were made based on the Bayesian surplus production (BSP) models (ISC BILLWG, 2009b). The 2014 swordfish stock assessment used the two-stock hypothesis to assess the stock, but only used BSP models because it was an update and not a benchmark assessment and did not incorporate the length frequency data available primarily from pooled-sex swordfish samples (ISC BILLWG, 2014). Likewise, the 2010 IATTC swordfish stock assessment in the eastern Pacific did not incorporate length frequency data and based management recommendations on the results of the BSP assessment models (IATTC SAC, 2011).

Other research on the Hawaiian Longline length frequency data has suggested that the data collected contain information on the sexual dimorphism known to occur in swordfish growth (DeMartini *et al.* 2007, Brodziak and Courtney 2009). However, questions remained about whether the sample size was large enough to capture those effects and if differences between mean sizes really suggested sexual dimorphism. In 2009, the ISC Billfish Working Group (WG) suggested a two-gender stock assessment model could provide a better approximation of swordfish population dynamics for future assessments, but noted that this would be difficult due to the lack of sex-specific length frequency data and a lack of information on the spatial patterns of swordfish size composition through time. This working paper presents an analysis of the length frequency data available from the Pacific Islands Regional Observer Program database on the Hawaiian longline fishery by fishery sector (deep-set and shallow-set), sex (males/females), and maturity (adults/juveniles) using generalized additive models. In particular, our goal is to develop predictive models to describe the spatial and temporal patterns in swordfish size composition by gender and also for immature and mature fish.

Methods

Eye-fork length data were analyzed from the Pacific Islands Region Observer Program database on the Hawaiian longline fishery (Accessed 31 March 2017), which included records from 1994 to 2016. A total of 110,192 lengths were available representing landings in both the shallow-set swordfish targeting (< 15 hooks per float) and the deep-set tuna targeting (≥ 15 hooks per float) sectors of the fishery (Walsh and Brodziak, 2015). The deep-set sector also incidentally catches

swordfish. The deep-set and shallow-set data were analyzed separately here due to the differences in spatial distributions and targeting of species between the two fleets, which would result in any sector-effect being confounded with the spatial parameters. The shallow-set fishing activity has primarily occurred in high latitudes (>30°N) during the first and fourth quarters of the year. The deep-set fishing activities occur year round and extend to the equator (Walsh and Brodziak, 2015).

Due to interactions with protected sea turtles, the shallow-set swordfish fishery was closed from February 2001 to May 2004 (Gilman *et al.*, 2007). During this time many vessels targeting swordfish began targeting tuna. A second closure occurred from March to December 2006 when the Hawaii-based shallow-set longline fishery for swordfish reached the annual limit for interactions with loggerhead sea turtles (NMFS, 2017). There have been several changes to the reporting regulations in PRIOP since its onset in 1994 (Pacific Islands Region Office, 2017). Observer coverage varied significantly prior to 2000, with observer coverage between 3.3 and 10.4 % for the entire fishery (NMFS, 2017). Starting in 2001, the observer program had a target of 20% observer coverage on deep-set longline vessels and mandatory 100% observer coverage on shallow-set longline vessels. Prior to 2006 observers measured every billfish caught. Since 2006, observers measured every third fish caught, regardless of species. Therefore the proportion of swordfish measured in the catch decreased after 2006 but the total number of swordfish measured increased due to increased observer coverage (Figure 1).

The longline data were aggregated by year, month, and 1° × 1° spatial grids for analysis. A hierarchical cluster analysis was used to identify any significant clusters by month for each fishing sector. Clustering was performed using the dissimilarity between each data cluster or data point with distances recomputed using the Lance-Williams dissimilarity update formula for the complete linkage method in order to reduce the number of parameters estimated in the model. The months included in each cluster were determined by cutting the tree into 2, 3, or 4 clusters and evaluating if the data points grouped by month into clusters. The analysis for the deep-set sector suggested using two clusters: cluster one including the fall and winter months August-March; cluster two including April, May, June, and July. It is notable that cluster one corresponds to the spawning season for North Pacific swordfish (Sun *et al.*, 2002). The analysis for the shallow-set sector suggested a single cluster for all months. The models used to analyze the data included a factor for the two clusters for the deep-set data and, lacking any apparent higher-level structure, a factor for each month for the shallow-set sector.

Fish were classified into adults and juveniles by assuming all fish over the length at which 50% of the population reaches maturity (L_{50}) were adults. The female L_{50} is 143 cm and male L_{50} is 102 cm (DeMartini *et al.*, 2007). Fish below the L_{50} for their respective sex were classified as juveniles. Approximately 50% of the measured swordfish included in the analyses were sexed, with unsexed fish (labeled as U) primarily smaller fish which are presumably harder to sex (Figure 2). All unsexed fish under 102 cm were classified as juvenile and over 143 cm were classified as adults. For unsexed fish between 102 and 143 cm, the probability of being an adult given that the fish was unsexed was assumed to be equal to the probability that the fish was male. The probability of being male was calculated by estimating the age of a fish at length in two cm increments using the standard von Bertalanffy growth curve with sex-specific parameters from DeMartini *et al.* (2007). Then the natural mortality at age was defined as the mean of 5

natural mortality estimation methods recommended previously by the WG: the Hoenig (1983), Alverson and Carney (1975), Pauly (1980), and Beverton-Holt invariant 2 (Jensen 1996), and the Lorenzen (1996) tropical system estimator (Brodziak 2009, ISC BILLWG 2009a). The probability of being male at size was then calculated using the number of males and females remaining at each size assuming an initial 1:1 male-to-female ratio.

Generalized additive models (GAMs) were used to quantify the effects of spatial, temporal, and environmental variables on swordfish lengths. Variables explored in the analysis were latitude and longitude, sea surface temperature (SST°C), the Pacific Decadal Oscillation Index (PDO), and the Southern Oscillation Index (SOI). For deep-set models cluster was included as a by variable in the 2D smooth for latitude and longitude. This produces a smooth for each level of the by factor variable (Wood, 2006). Year, gender, and month or cluster were explored as factors. Sea surface temperatures were monthly mean values measured by the AVHRR Pathfinder satellite downloaded from NOAA OceanWatch with 0.1° resolution. The Pacific Decadal Oscillation index and Southern Oscillation Index were obtained from the NOAA National Centers for Environmental Information (NOAA NCDC, 2017). Correlation coefficients between the environmental and spatial covariates and eye-fork length for each sector are in Table 1. All correlation coefficients were statistically different from zero ($p<0.05$) according to Pearson's product-moment correlation except for those four indicated by superscript "^".

GAMs were run in R version 3.3.2 using the mgcv package (Wood, 2006, R Core Team, 2016). Ten different GAMs were run on various subsets of the data using thin plate regression splines for the smooth functions and a Gaussian link function (e.g., Wood 2006). Of the ten different GAMs, 5 were fit using subsets of the deep-set data and 5 were fit using subsets of the shallow-set data (Table 2). For the deep-set sector, the 5 GAMs were fit to all samples (model D1), females only (model D2), males only (model D3), adults only (model D4), and juveniles only (model D5). Analogous GAMs were fit for the shallow-set sector (models S1 to S5). The longline observer data from each sector were analyzed separately and also broken into male/female and adult/juvenile fish to explore differences between each subset of data. Final GAMs were determined using a forward stepwise selection process based upon the percent deviance explained and the generalized cross validation score (GCV). The GCV is an estimate of the degree of smoothness for the GAM model penalized for overfitting the data, functioning similarly to an AIC value for model selection (Wood, 2006). Explanatory variables were ordered based on the highest percent deviance and the lowest GCV score.

Only swordfish which were assigned a gender in the fishery observer database were included in the male and female GAMs. For the adult and juvenile GAMs multiple iterations of the classification method was employed to include the uncertainty around unsexed fish in the adult and juvenile GAMs. The final model used was selected using the same process as described for the rest of the models using a single data set with the additionally classified fish. This final model was then used to fit 500 iterations of the classified adult and juvenile data sets and averaged across all models (Crane-Droesch *et al.*, 2013). The model-averaged parameter vector was calculated as the arithmetic average of the individual parameters from the M imputation models as:

$$\hat{\beta} = \frac{1}{M}\sum_{m=1}^{M}\hat{\beta}_m$$

Where $\hat{B}_m$ is the parameter estimates from each of M models. The covariance matrix ($\hat{V}_{\hat{\beta}}$) of the estimated parameters was calculated as the average of the individual covariance matrices of the M imputation models plus a correction matrix that accounts for the covariation among the models as:

$$\hat{V}_{\hat{\beta}} = W + \left(1 + \frac{1}{M}\right)B \quad (1)$$

where

$$B = \frac{1}{M-1}\sum_{m=1}^{M}(\hat{\beta}_m - \hat{\bar{\beta}})(\hat{\beta}_m - \hat{\bar{\beta}})^T, \quad (2)$$

$$W = \frac{1}{M}\sum_{m=1}^{M}\widehat{VCV}_m, \quad (3)$$

$\hat{B}_m$ is the parameter estimates from each of M models, $\hat{\bar{\beta}}$ is the mean parameter estimate, and $\widehat{VCV}$ is the estimated variance-covariance matrix of the estimated parameters. This inflates the standard errors on coefficients which are relatively less certain due to the missing data (Crane-Doresch *et al.*, 2013).

Results

Data Summary

Average mean length of swordfish did not vary significantly over time in neither the deep-set (Figure 3 top panel) nor the shallow-set (bottom panel) longline sector. Annual mean lengths in the deep-set sector were small and more variable, with smaller fish caught in the 1990s and larger fish caught in the 2010s (Figure 3, top panel). Mean length peaked in the deep-set sector in 2008 at 139cm, and decreased to around 115 cm in the last three years of the analysis. Prior to 2008, mean lengths were generally less than 100cm and more similar to the overall median length of 82 cm. Mean length in the shallow-set sector was very stable, with annual mean lengths between 140 and 150 cm every year, in line with the overall median length of 145 cm (Figure 3, bottom panel). Maps of mean length by set also show the significant difference in the size of fish caught in the deep- and shallow-set sectors (Figure 4). Deep-set sector catches were smaller and skewed right with a mean length of 102 cm and median length of 82 cm. The shallow-set sector catches larger fish overall, and the catches were more normally distributed with the mean and

median lengths 145 cm. There were more sets observed and more fish measured in the shallow-set sector than in the deep-set sector (Figure 5).

There were clear trends in the mean length of swordfish caught in both fisheries throughout the year. The smallest fish were caught in August through November around the Hawaiian Islands, with the minimum mean length occurring in September at 87 cm, compared to the maximum mean length occurring in January at 151 cm (Figure 6). You can see the large influx of small fish in August and September from the peaks in the density histograms around 70 and 80 cm in Figure 7. This might be a recruitment signal as most of the small fish caught were likely young of the year and appear shortly after the spawning season. The largest fish were caught in the northernmost part of the fished area. In April – July the large fish were also caught around the Hawaiian Islands, which coincides with the swordfish spawning season. Larger fish were also caught in the northeastern areas of the fishery when comparing catches between female and male swordfish (Figure 8). Male swordfish, however, were smaller on average than female fish with median lengths of males (142 cm) about 14 cm smaller than females (156 cm). This difference in size between male and female swordfish has been described previously (Brodziak and Courtney, 2008) and evidence for sexual dimorphism has been found in both the length frequency data and in age-length curves (DeMartini *et al.,* 2007).

Generalized Additive Models

Ten different sets of GAMs were run with various subsets of the length frequency data, divided by sex, set, and maturity. Final models and the amount of deviance explained are in Tables 2 and 3. The explanatory variables included explained more of the deviance in the deep-set sector than in the shallow-set sector. The spatial component and year effect were the explanatory variables that explained the majority of the deviance for most of the models and cluster was an important variable for the deep-set models. The environmental variables explained less deviance, but some interesting patterns were apparent. Overall, the correlations between the environment variables were relatively low but significantly different from zero (Table 1). SST was more correlated with latitude and longitude in the shallow-set sector than in the deep-set sector. PDO and SOI were also moderately correlated with each other (−0.47 shallow, −0.46 deep). Correlations between SST and PDO/SOI were generally less than 0.15. Diagnostic plots for each of the GAMs can be found in Appendix 1.

Deep-set Sector

For model D1 using all the length data, the final model explained 49% of the deviance with the cluster, spatial component, and gender explaining the majority of the deviance. SST explained more deviance than year, and SOI and PDO only contributed to 3% of the deviance explained each. The partial effect of SST on length showed the largest fish were caught at SSTs around 20°C with a decrease in lengths with increased temperatures (Figure 9). The length of swordfish caught increased with more positive PDO indices (which correspond to cooler waters around Hawaii) and the smallest fish were caught in time periods where the SOI was −2 and the largest fish caught in time periods where the SOI was −1. As the SOI became more positive the lengths gradually decreased. The maps of the predicted lengths in the fishing area shows much larger fish throughout the entire area during cluster 2 (April – July) compared to the rest of the year (Figure 10). The smallest fish in cluster two were found south of 10°N while the largest fish were centered around 20°N 155°W.

When the data were analyzed as female and male separately in models D2 and D3, respectively, some evidence of differences between the sexes appears. Much more deviance was explained by the final model for model D2 (43%) than for model D3 (29%) and different environmental factors have greater explanatory power (Table 2). The climatological variables PDO and SOI had more explanatory power for female lengths while SST had a higher explanatory power for male lengths. For females, larger fish were caught with more positive PDO, while the largest sizes were caught around a SOI of 1.75 (Figure 11). For males, the climatological parameters were not significant and were not included in the final model, however fish length increased with increasing temperature (Figure 12). There were some differences in spatial distribution between the male and female lengths caught in the deep-set sector. In cluster one, the smallest fish of both sexes were located between 15°-25°N with the smallest females centered around 155°W but males showing two clusters of small fish around 165°W and 155°W (Figures 13 and 14, top panel). The largest fish of each sex were found in different areas. Large females were caught in the northwest and large males were caught in the northeast. In cluster two the largest fish were caught between 15°N and 25°N for both sexes, but the smaller fish were in different areas (Figures 13 and 14, bottom panel). Small males were caught in the northeast and small females were caught in the south.

For the mature swordfish model D4, approximately 32% of the deviance was explained with gender, spatial component, and cluster explaining the majority of the data. SOI was not a significant explanatory variable and was not included in the model and Year, SST, and PDO all explained less than 5% of the deviance each. Since the models D4 and D5 were averaged after 500 model imputations, the percent deviance explained presented in Table 2 were only approximate and based off of a single run, however model runs in general had very similar results. The SST smooth function had a large confidence interval due to the model averaging, but generally the trend was fairly flat with slightly larger fish at colder temperatures and warmer temperatures. Fish size also increased with more positive PDO indices (Figure 15). The spatial distribution of the predicted lengths show in cluster 1 the fish caught were generally smaller than in cluster 2 and these smaller fish were centered around 20°N 155°W with larger fish caught in the southeast (Figure 16). In cluster 2, the largest fish were caught between 20°N and 30°N with the smaller fish caught in the south.

In comparison, for the immature swordfish model D5, approximately 34% of the deviance was explained, and the spatial component and SST explained the majority of the deviance. The smooth function for SST shows that the largest juveniles were caught in waters where the SST was around 20°C and smaller in cooler and warmer water temperatures, however this function has very large confidence intervals (Figure 17). Juvenile fish size appears to increase with more positive PDO indices and the smooth function is fairly flat for the SOI, except for a slight increase in length at positive values. For both adult and juvenile fish, fish caught during cluster two (April – July) were significantly larger than those caught during the rest of the year. The spatial distribution of juvenile swordfish show the largest fish were caught in the northwestern area of the fishery during cluster one (Figure 18). In cluster 2, the largest fish are caught around 20°N with the smaller fish in the south.

Shallow-set Sector

For the all-samples data set, model S1 included six explanatory variables and only explained 11% of the deviance. Only gender explained more than 5% of the total deviance. The largest fish

were caught at SSTs between 15°C and 24°C with a decrease in lengths at temperatures warmer and cooler than this range (Figure 19). The length of swordfish caught was relatively flat between PDO indices of −2 and 0.5 with a peak in length occurring around 1.75 followed by a subsequent decrease. The partial effect of SOI on length showed the largest fish were caught in time periods where the SOI was less than −2 and relatively flat at more positive values of the SOI. The mean length of fish was relatively flat or slightly increasing until 2009 and decreased until 2016. The partial effect of month on the mean lengths show a fairly flat trend until July followed by a significant decrease in August, reaching a minimum in September and increase again until December. The predicted lengths spatial distribution shows that the largest fish were caught in the northeast and the smallest fish were caught in the southeast (Figure 20).

The majority of the deviance explained in model S1 was from the variable for gender so it is not surprising that very little deviance is explained when males and females are modeled separately. Less than 5% of the deviance was explained by the final model for females only model S2. Sea surface temperature was excluded from the model as it was not statistically significant. The partial effect of PDO on female lengths shows that larger fish are caught when the PDO index was less than −2, then was relatively flat between −2 and 1 (Figure 21). When PDO indices were more positive than 1 the eye-fork length of female fish caught decreases drastically. Female lengths gradually increase with more positive SOI. The mean length of female swordfish caught increased from 1994 to 2012, after which lengths decreased slightly until 2015. Large confidence intervals in 2003–2004 are due to the shallow-set sector closure. Unlike the males only model, mean length does not decrease throughout the year, but is relatively stable until July. In August and September mean lengths decrease significantly and are followed by a rapid increase through December. The spatial distribution of female predicted lengths is consistent with the male patterns (Figure 22). The largest fish were caught in the northeast and the smallest fish in the south.

For the males only model S3, almost 8% of the deviance was explained, which included all of the variables. The spatial component and year had the most explanatory power followed by SOI, PDO, SST, and month. Despite the low explanatory power, all of the variable were statistically significant. The partial effect of SOI and the PDO index on swordfish length were similar (Figure 23). The largest fish were caught when the SOI and PDO indices were less than −2. Between −1 and 3 the effect of SOI on length was fairly flat. The effect of the PDO index on length was an increase in lengths from −2 to 0, followed by a decrease in lengths as the index became more positive. The effect of SST on male swordfish length was similar to model S1, with peaks at around 17°C and 24°C. The mean lengths of males were highest after the closure but decreased from 2012–2015. The male lengths decreased throughout the year until September when the smallest fish were caught and increased again rapidly in October through December. The spatial distribution of predicted male swordfish lengths was also similar to the pooled shallow-set data, with the largest fish caught in the northeast and small fish caught in the southeast and south (Figure 24). Small males were also caught in the northwest.

For the adults only data, model S4 explained approximately 19% of the total deviance in the adult swordfish shallow-set sector data. Gender has the highest explanatory power, followed by the spatial component and year. SST was a better explanatory variable than the climatological variables PDO and SOI. The final model for model S2 had the same form as model S1, which is to be expected as more than 90% of the fish caught in the shallow-set sector were over 102 cm and 52% of the fish caught were over 143 cm. The partial effect of SST suggested that eye-fork

length increased with increased temperatures, although the smooth had a large confidence interval (Figure 25). The PDO index trend was fairly flat. The partial effect of the SOI suggested that larger fish were caught when the SOI was less than −2, but remains fairly flat between −1 and 3. The annual predicted mean length decreased initially until 1997, then increased slightly until the closure. After the closure the mean length increased until around 2011–2012, then it decreased again. In the monthly trend, mean length decreased from January to a minimum in September and then rapidly increased again through December. The spatial distribution shows that large fish were caught in the north and west of the fishing area, while the smallest fish were caught in the east (Figure 26).

In contrast, the immature swordfish model S5 had the highest deviance explained (23%) of all the shallow-set models, but was still smaller than any of the deep-set models. The variables with the most explanatory power were the same as for model S2, however SST had more explanatory power in the model than SOI and the PDO index. The partial effect of SST on the eye-fork length is similar to the juveniles caught in the deep-set sector characterized by a peak around 20°C and decreased lengths in warmer and cooler water temperatures (Figure 27). The confidence intervals for the juvenile averaged model was much smaller than those for the other averaged models. The partial effect of the SOI on eye-fork length has some interesting characteristics. The maximum lengths caught were when the SOI was around −2, after which lengths decreased. Between −1 and 1 the trend was relatively flat with a slight increase in length around 2 followed by a sharp decrease with more positive SOI. The PDO index partial effect showed a relative increase in swordfish lengths as the PDO became more positive. The mean length is fairly variable between 1994 and 2010, but decreased in 2011 and remained at a similar length through 2016. The monthly trend showed an increase in length from January to May-June followed by a decrease to a minimum in September and rapid increase again through December. The spatial distribution again showed the largest fish in the northeast, but the smallest fish were caught throughout the west and south of the fishing area (Figure 28).

Discussion

Our analysis shows notable size differences between the swordfish caught in the shallow-set and deep-set sectors. This trend is in agreement with the observed decrease in the number of small swordfish caught when the swordfish fishery was expanding as a part of the fleet switched from targeting tuna to targeting swordfish (DiNardo and Kwok, 1998). The deep-set sector catches fewer swordfish and the majority of these fish are small and less than one year old.

The seven variables explored for the shallow-set sector GAMs did not explain very much of the deviation in the data. There is not a substantial amount of variability in the annual mean length of the swordfish caught in the shallow-set sector. One explanation for this pattern is fishery targeting. In particular, the low variability in mean length in the shallow-set sector suggests that since the shallow-set sector targets swordfish specifically, fishermen may be making decisions about when and where to fish based on their knowledge to target the largest swordfish. These decisions may already account for some of the environmental variables used in these models. For example, spatial patterns in the effort for the shallow-set sector clearly show that fishing occurs in more northern latitudes, where larger fish and cooler SST are found and the spatial covariate of the GAMs explained a majority of the deviance in the data. The correlation between SST and latitude was -0.47, suggesting that the spatial component of the model already accounted for some of the variability due to SST. Including details about the fishing operations such as vessel,

captain, or gear configurations such as number of lightsticks per hook or lunar light levels which may relate to the effectiveness of the fishing gear may increase the amount of deviance explained (Bigelow *et al.,* 1999). Also, fishermen may be specifically targeting the areas where large swordfish are caught, and therefore the assumption of a random distribution of fishing effort is not accurate (Chang *et al.*, 2013). The environmental variables are based on the location of the start of the set and, for SST, are daytime temperatures averaged over a month, however the longline gear can be 48-64 km in length and are only set at night for 6–10 hours (Bigelow *et al.,* 1999). This can stretch across frontal boundaries where there are rapid changes in SST and are areas where swordfish are known to aggregate (Sakagawa, 1989) including the subtropical frontal zone between 27° and 33°N and subarctic frontal zone between 41° and 43°N, which bounds the primary fishing area for the shallow-set sector. These zones can have fairly weak SST gradients but strong halocline gradients but are known to be areas where swordfish catch is higher (Bigelow *et al.,* 1999). This is likely less of a response to the SST gradient and more because these frontal zones are usually productive and good sources of prey (Bakun, 1996). Other analyses of the relationship between CPUE and SST have not suggested any preferred temperatures for swordfish in the Atlantic (Santos *et al.,* 2006) Our analysis with only SST data may be unable to capture these dynamics in the analysis and other indicators of frontal zone characteristics such as salinity, SST frontal energy, or sea surface height anomaly may have more explanatory power (Bigelow *et al.,* 1999).

The deep-set sector data was more variable overall than the shallow-set sector likely because swordfish are not targeted but are caught incidentally. There was much less correlation between the covariates explored for the deep-set sector which help may explain why the deep-set GAMs had a higher percent deviance explained. Despite evidence showing that SST can explain around 40% of the variance in CPUE data for swordfish (Bigelow *et al.,* 1999, Chang *et al.,* 2013, Hsu *et al.,* 2015) it did not explain a large percentage of the deviance in the length frequency data of the deep-set sector. Even when the spatial components were excluded from the model, SST only explained up to 10% of the variability of the deep-set sector data and 3% of the variability of the shallow-set sector data. In the deep-set sector, this may be because deep-set gear are set during the day at between 150–400m in depth, so the SST may not be an accurate representative of what is happening at depth (Bigelow *et al.,* 1999). Swordfish are known to follow their diurnally migrating prey, therefore the deviance may be better explained by factors such as mixed layer depth or temperature at depth where swordfish are vulnerable to the gear (Chang *et al.,* 2013). This likely would not increase the amount of deviance explained in the shallow-set fishery, as longlines are typically set within the mixed-layer where SST is assumed to be similar to the temperature at depth. Ultimately, the mismatch between SST's power to explain variability in CPUE and SST's power to explain variability in swordfish length suggests that there may be different mechanisms controlling the length composition of swordfish catches than those controlling the CPUE.

For both sectors, SST was not a significant covariate for females but it was for males. Since there is a fairly low correlation between SST and PDO or SOI (<0.1) there may be different dynamics driving male and female distributions by size. Spatial differences between the sexes are minimal. However, it should be noted that only about 50% of the individuals measured are sexed, the majority of these sexed individuals are large, and none of the environmental variables contribute

to a large proportion of the deviance explained. Therefore the results of the male and female GAMs may not be representative for all size classes of swordfish.

Overall, the analysis shows that spatial and temporal variation had significantly more influence on swordfish length than the environmental variables. For the deep-set sector, intra-annual temporal variation also was an important covariate. Data from both sectors contain important information on the spatial variation of swordfish by length although additional work is necessary to better explain the length variation in the shallow-set sector. It may also be useful to include length data from other swordfish-targeting longline fisheries. This would expand the spatial coverage of the analysis and help determine if there are North Pacific-wide patterns in swordfish lengths. Like previous conclusions about the CPUE index (ISC BILLWG, 2009a), these results suggest that the size compositions of catches in the deep-set sector are not representative of the exploited stock, however they may have potential use as a recruitment index.

References

Alverson, D., and M. Carney. 1975. A graphic review of the growth and decay of population cohorts. Journal du Conseil International pour l'Exploration de la Mer. 36(2):133-143.

Bakun, A. 1996. Patterns in the ocean: Ocean processes and marine population dynamics. California Sea Grant College, National Oceanic and Atmospheric Administration, 323 pp.

Bigelow, K. A., C. H. Boggs and X. I. He. 1999. Environmental effects on swordfish and blue shark catch rates in the US North Pacific longline fishery. Fisheries Oceanography 8(3): 178-198.

Brodziak, J. 2009. Potential Natural Mortality Rates of North Pacific Swordfish, *Xiphias gladius*. ISC/09/BILLWG-1/13.

Brodziak, J. and D. Courtney. 2008. Length Distributions of Female and Male Swordfish, *Xiphias gladius*, Captured in the Directed Hawaii Pelagic Longline Fishery during 1994-2008. ISC/09/BILLWG-1/07.

Chang, Y.-J., C.-L. Sun, Y. Chen, S.-Z. Yeh, G. DiNardo and N.-J. Su. 2013. Modelling the impacts of environmental variation on the habitat suitability of swordfish, Xiphias gladius, in the equatorial Atlantic Ocean. ICES Journal of Marine Science 70(5): 1000-1012.

Crane-Droesch, A., S. Abiven, S. Jeffery and M. S. Torn. 2013. Heterogeneous global crop yield response to biochar: a meta-regression analysis. Environmental Research Letters 8(4): 044-049.

DeMartini, E. E., J. H. Uchiyama, R. L. Humpreys Jr., J. D. Sampaga and H. A. Williams. 2007. Age and growth of swordfish (*Xiphias gladius*) caught by the Hawaii-based pelagic longline fishery. Fishery Bulletin 105: 356-367.

DiNardo G.T. and W. Kwok. 1998. Spatiotemporal dynamics of swordfish, *Xiphias gladius*, landings in the Hawaii-based North Pacific pelagic longline fishery. Barrett, Isadore, Oscar Sosa-Nishizaki, and Norman Bartoo (eds.). *Biology and fisheries of swordfish, Xiphias gladius. Papers from the International Symposium on Pacific Swordfish, Ensenada, Mexico, 11-14 December 1994*. U.S. Dep. Commer., NOAA Tech. Rep. NMFS 142, 51-64.

Gilman, E., D. Kobayashi, T. Swenarton, N. Brothers, P. Dalzell and I. Kinan-Kelly. 2007. Reducing sea turtle interactions in the Hawaii-based longline swordfish fishery. Biological Conservation 139(1–2): 19-28.

Hoenig, J. 1983. Empirical use of longevity data to estimate mortality rates. Fish. Bull. 82:898-903.

Hsu, A. C., A. M. Boustany, J. J. Roberts, J.-H. Chang and P. N. Halpin. 2015. Tuna and swordfish catch in the U.S. northwest Atlantic longline fishery in relation to mesoscale eddies. Fisheries Oceanography 24(6): 508-520.

IATTC SAC. 2011. Status of Swordfish in the Eastern Pacific Ocean in 2010 and Outlook for the Future. Inter-American Tropical Tuna Commission Scientific Advisory Committee. Document SAC-02-09. 9-12 May 2011. La Jolla, California, USA.

ISC BILLWG. 2009a. Report of the billfish working group workshop. International Scientific Committee for Tuna and Tuna-like Species in the North Pacific Ocean 3-10 February 2009. Honolulu, Hawaii, USA.

ISC BILLWG. 2009b. Report of the billfish working group workshop (Annex 7). International Scientific Committee for Tuna and Tuna-like Species in the North Pacific Ocean 19-26 May 2009. Busan, Korea.

ISC BILLWG. 2014. North Pacific Swordfish (*Xiphiaus gladius*) Stock Assessment in 2014. International Scientific Committee for Tuna and Tuna-like Species in the North Pacific Ocean 16-22 July 2014. Taipei, Chinese-Taipei.

Jensen, A. 1996. Beverton and Holt life history invariants result from optimal trade-off of reproduction and survival. Can. J. Fish. Aquat. Sci. 53:820-822.

Lorenzen, K. 1996. The relationship between body weight and natural mortality in juvenile and adult fish: a comparison of natural ecosystems and aquaculture. J. Fish. Biol. 49:627-647.

NMFS. 2017. Hawaii longline fishery logbook statistics -non-confidential summary tables. Available online at http://www.pifsc.noaa.gov/fmb/reports.php, accessed 8 May 2017. National Marine Fisheries Service, Pacific Islands Fisheries Science Center, Honolulu.

NOAA NCDC. 2017. Spatially and temporally large-scale anomalies that influence the variability of the atmospheric circulation. Online Database https://www.ncdc.noaa.gov/teleconnections/ Accessed 31 March 2017.

Pauly, D. 1980. On the interrelationships between natural mortality, growth parameters, and mean environmental temperature in 175 fish stocks. Journal du Conseil International pour l'Exploration de la Mer. 39(2):175-192.

Pacific Islands Region Office (PIRO). 2017. Hawaii Longline Observer Program Observer Field Manual. Version LM.17.02. National Oceanic and Atmospheric Administration, Pacific Islands Region, Honolulu, Hawaiʻi.

R Core Team. 2016. R: A language and environment for statistical computing. R Foundation for Statistical Computing, Vienna, Austria. URL https://www.R-project.org/.

Sakagawa, G.T. 1989. Trends in fisheries for swordfish in the Pacific Ocean. In: *Second International Billfish Symposium Proc., Part 1: Fishery and Stock Synopses, Data Needs and Management.* R.K. Stroud (ed.). Savannah, Georgia: National Coalition for Marine Conservation, Inc., pp. 61-79.

Santos, A.M.P., A.F.G. Fiúza and R.M. Laurs. 2006. Influence of SST on catches of swordfish and tuna in the Portuguese domestic longline fishery, International Journal of Remote Sensing, 27:15, 3131-3152.

Sun, C.-L., S.-P. Wang and S.-Z. Yeh. 2002. Age and growth of the swordfish (Xiphias gladius L.) in the waters around Taiwan determined from anal-fin rays." Fishery Bulletin 100: 822-835.

Walsh, W. A. and J. Brodziak. 2015. Billfish CPUE standardization in the Hawaii longline fishery: Model selection and multimodel inference. Fisheries Research 166: 151-162.

Wood, S.N. 2006. Generalized additive models: An introduction with R. Chapman & Hall, Boca Raton. 392 p.

Table 1. Correlation coefficients for the spatial and environmental covariates and eye-fork length for the deep- and shallow-set datasets. ^ indicates correlations not significantly different from zero.

Shallow-set

	Latitude	Longitude	PDO	SOI	Eye-Fork Length
SST	-0.49	-0.35	0.04	-0.12	-0.09
Latitude		0.57	-0.25	0.14	0.13
Longitude			-0.004^	0.01	0.11
PDO				-0.47	-0.11
SOI					0.06

Deep-set

	Latitude	Longitude	PDO	SOI	Eye-Fork Length
SST	0.06	0.21	–0.10	–0.10	–0.17
Latitude		0.43	–0.05	0.02^	0.0004^
Longitude			–0.02	–0.07	–0.11
PDO				–0.46	0.13
SOI					–0.02^

Table 2. Percent deviance explained by each predictor and the total deviance explained by the final model for each data set. NA = not applicable. ^ indicates parameters which were not statistically significant.

Model	Percent Deviance Explained								
	Cluster	Month	Year	Spatial (Lat*Lon)	Sex	SST	PDO	SOI	Total
All Deep (D1)	26%	NA	8%	18%	20%	11%	3%	3%	49%
Female Deep (D2)	29%	NA	12%	15%	NA	10%^	3%	8%	43%
Male Deep (D3)	16%	NA	8%	16%	NA	5%	0.5%^	3%^	29%
Adult Deep (D4)	8%	NA	3%	7%	27%	5%	2%	2%^	32%
Juvenile Deep (D5)	5%	NA	5%	11%	13%	10%	4%	2%	34%
All Shallow (S1)	NA	2%	2%	3%	6%	1%	0.8%	1%	11%
Female Shallow (S2)	NA	1%	2%	2%	NA	0.6%^	0.9%	0.4%	4%
Male Shallow (S3)	NA	3%	3%	4%	NA	1%	3%	1%	8%
Adult Shallow (S4)	NA	1%	2%	2%	17%	0.6%	1%	0.6%	19%
Juvenile Shallow (S5)	NA	3%	3%	6%	17%	3%	0.5%	1%	24%

Table 3. Final GAMs selected for each data set. See Table 2 for key to model names.

	Final Model Structure	GCV
D1	Length ~ Cluster+ s(Lat*Lon)+Sex+ s(SST) + Year+ s(PDO) + s(SOI)	1029.8
D2	Length ~ Cluster + s(Lat*Lon) + Year + s(SOI) + s(PDO)	1181.7
D3	Length ~ Cluster + s(Lat*Lon) + Year + s(SST)	1076
D4	Length ~ Sex + s(Lat*Lon) + Cluster + Year + s(PDO) + s(SST)	678.65
D5	Length ~ s(Lat*Lon) + s(SST) + Sex + Year + Cluster + s(PDO) + s(SOI)	338.8
S1	Length ~ Sex + s(Lat*Lon) + Year + s(SST)+ s(PDO)+ s(SOI) + Month	872.57
S2	Length ~ s(Lat*Lon) + Year + s(PDO) + s(SOI) + Month	872.37
S3	Length ~ s(Lat*Lon) + Year + s(SOI) + s(PDO) + s(SST) + Month	630.83
S4	Length ~ Sex + s(Lat*Lon) + Year + s(SST)+ s(PDO)+ s(SOI) + Month	580.72
S5	Length ~ Sex + s(Lat*Lon) + Year + s(SOI)+ s(PDO)+ s(SST) + Month	316.93

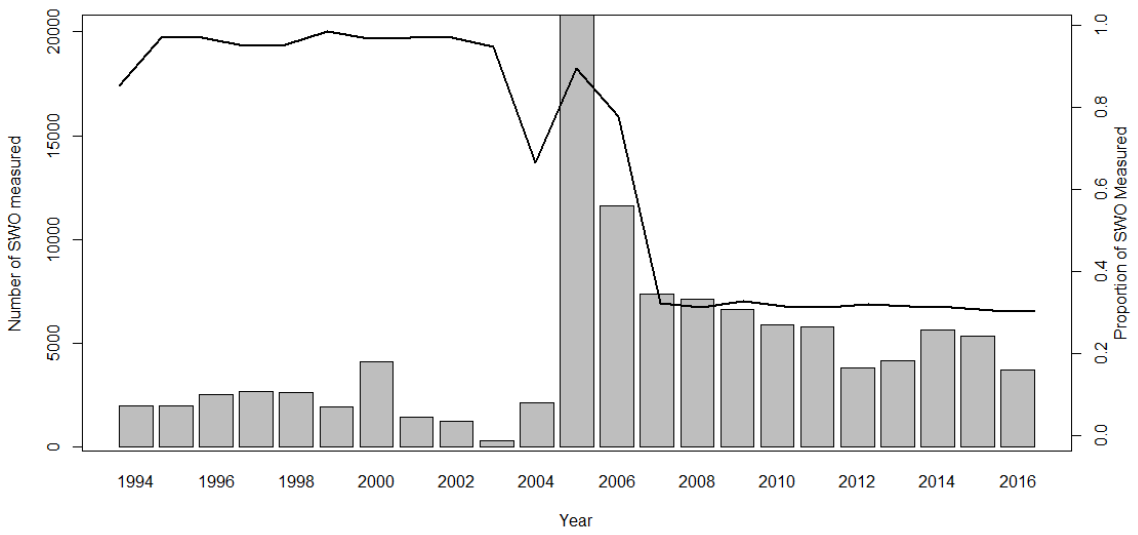

Figure 1. Proportion of swordfish measured (line, right axis) and total number of swordfish measured (histogram, left axis) in the catch by year in the Pacific Islands Regional Observer Program database on the Hawaiian longline fishery.

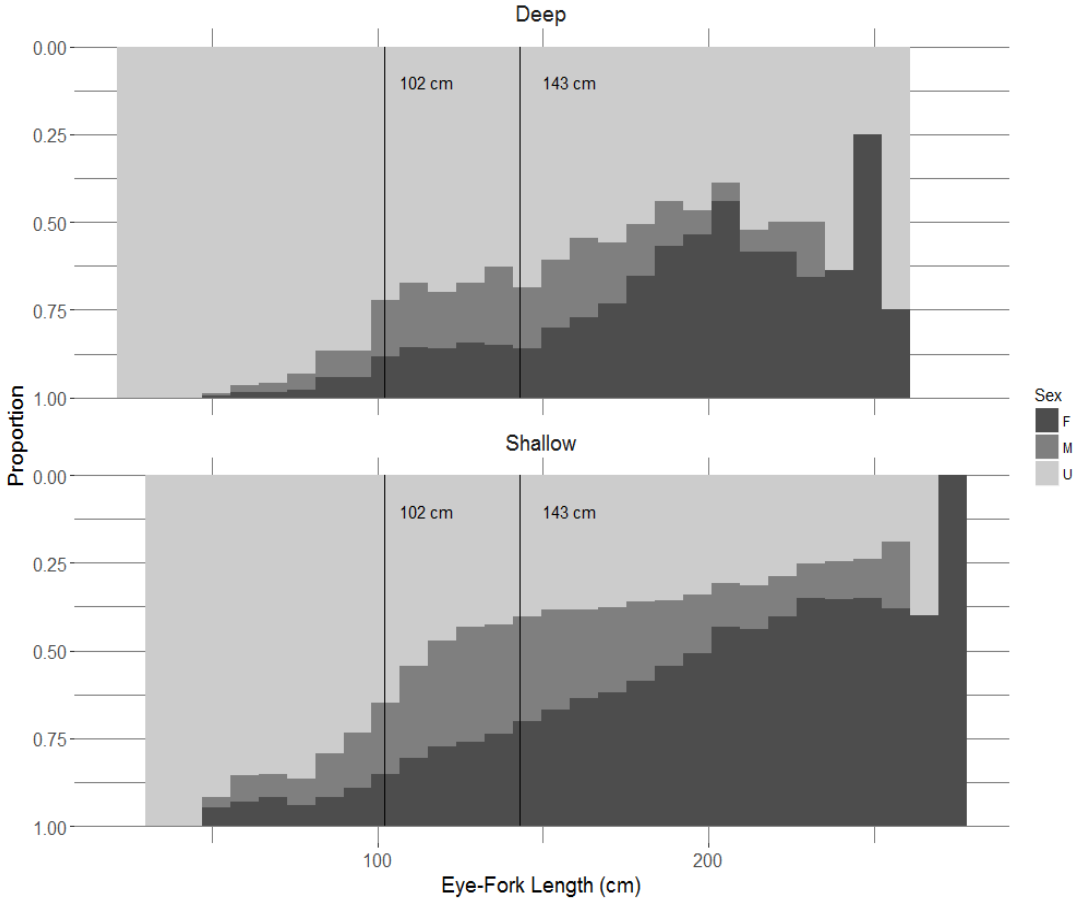

Figure 2. Proportion of fish measured that are sexed for the deep-set (top panel) and shallow-set (bottom panel). Black vertical lines indicate male L_{50} of 102 cm and female L_{50} of 143 cm.

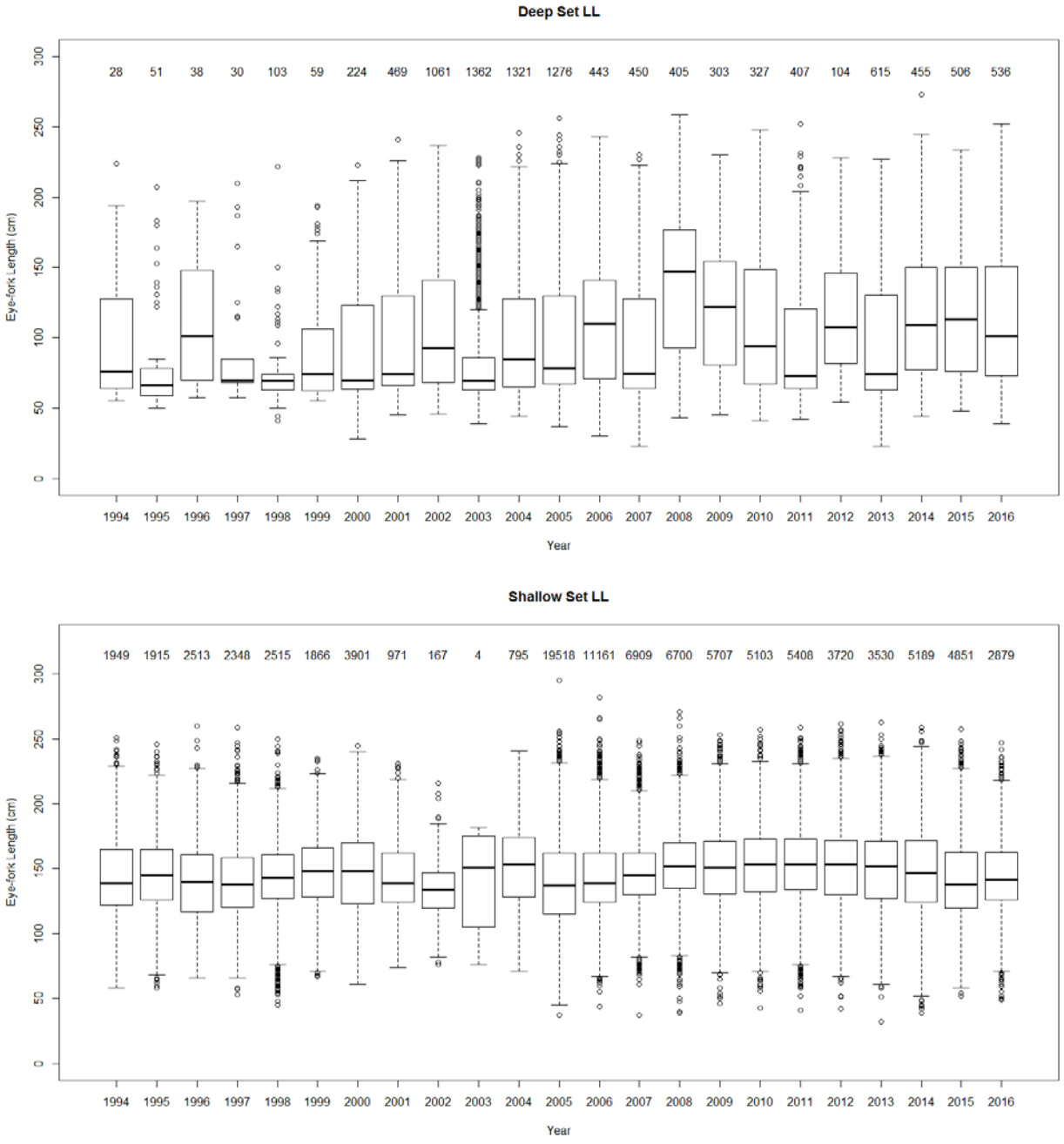

Figure 3. Box plot of swordfish lengths by year in 1994–2016 for the deep-set (top panel) and shallow-set (bottom panel) sector showing the median (solid black line) and quartiles (closed box). The whiskers show 1.5 times the interquartile range from the box and points indicate data outside of that range. Values above the boxes indicate the number of samples in each year.

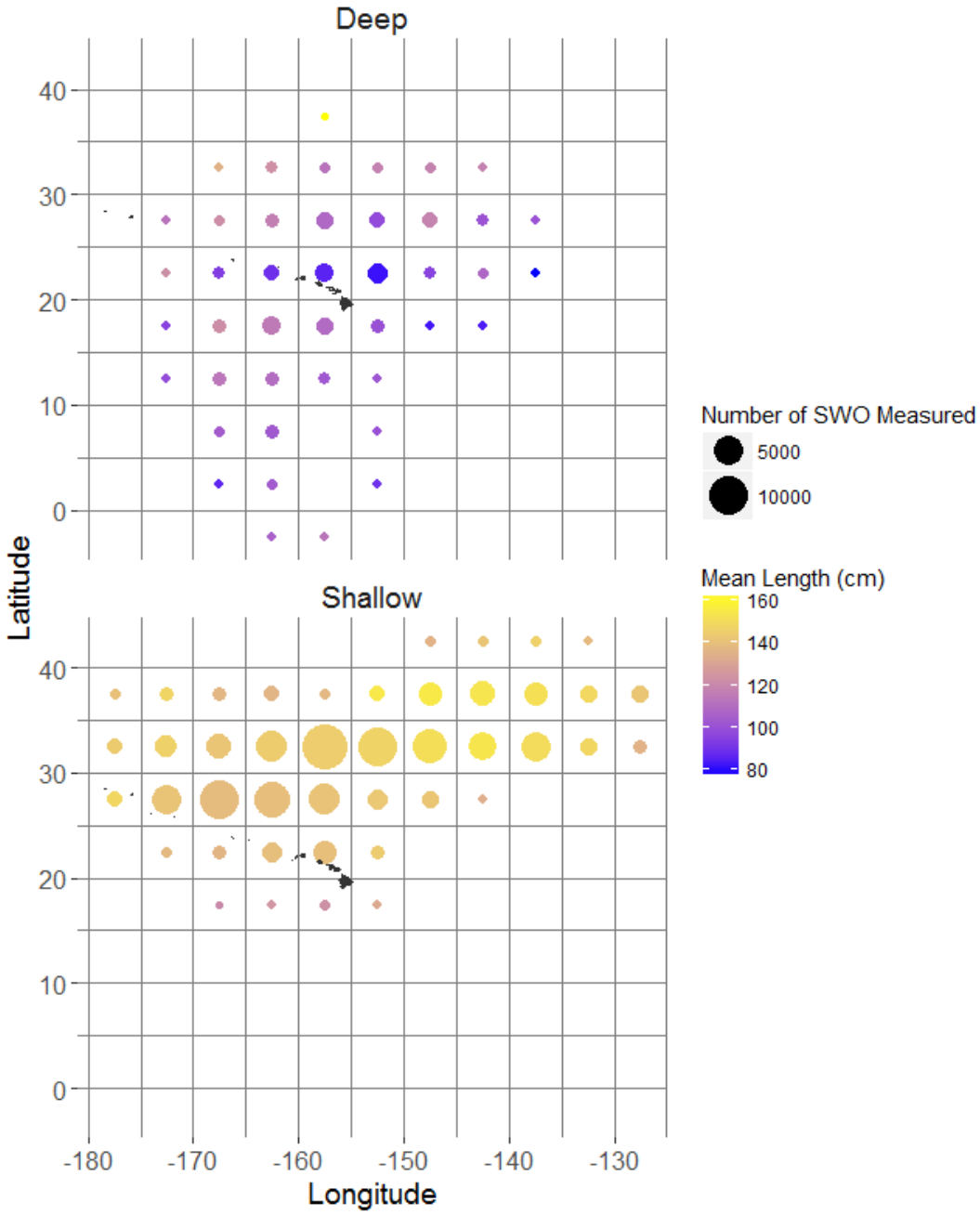

Figure 4. Spatial distribution of mean length in 5° × 5° squares for the deep-set sector (top panel) and shallow-set sector (bottom panel plotted over the Hawaiian Archipelago.

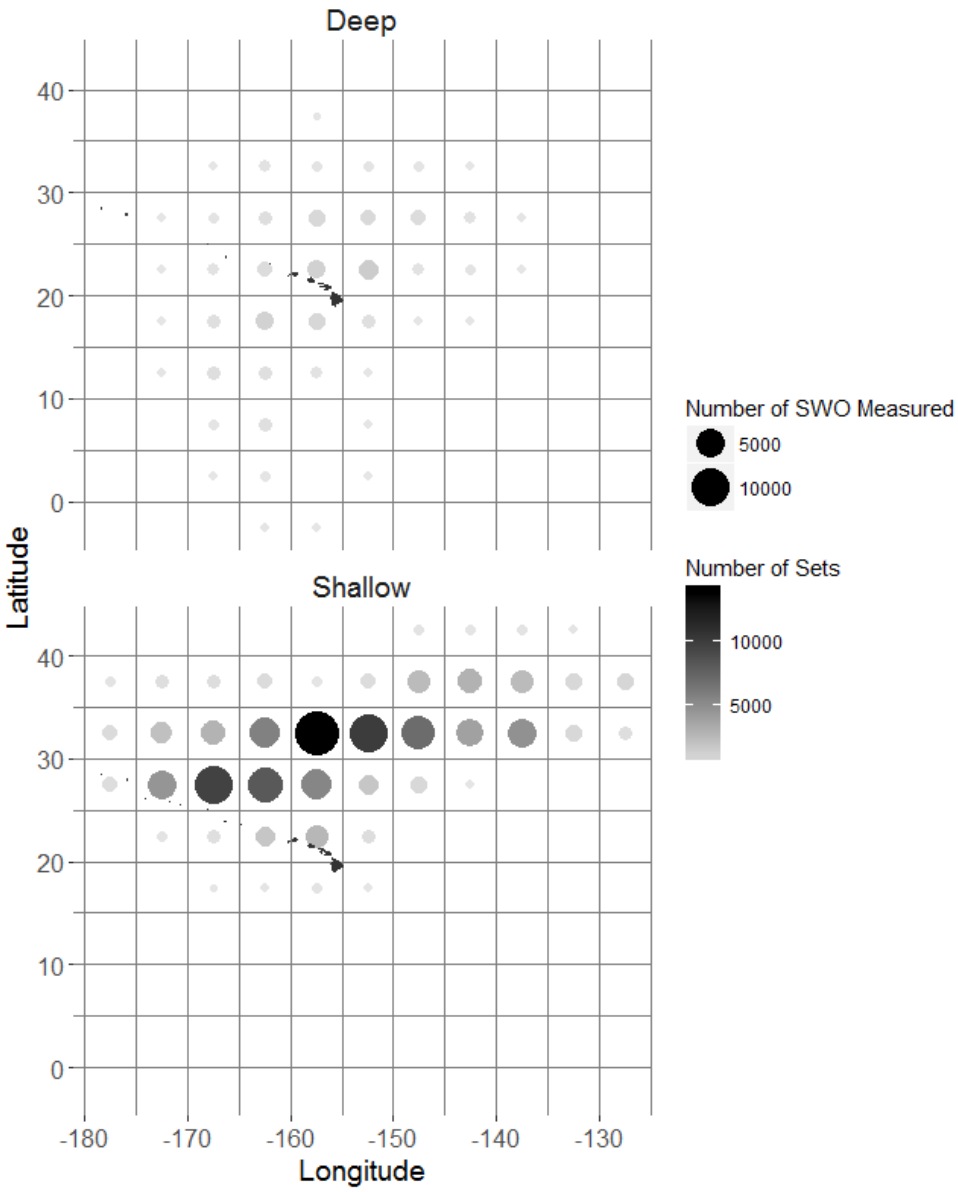

Figure 5. Number of swordfish measured (size of circle) and number of sets (color) for the deep-set (top panel) and shallow-set (bottom) sectors of the Hawaiian Longline fishery by 5° × 5° squares plotted over the Hawaiian Archipelago.

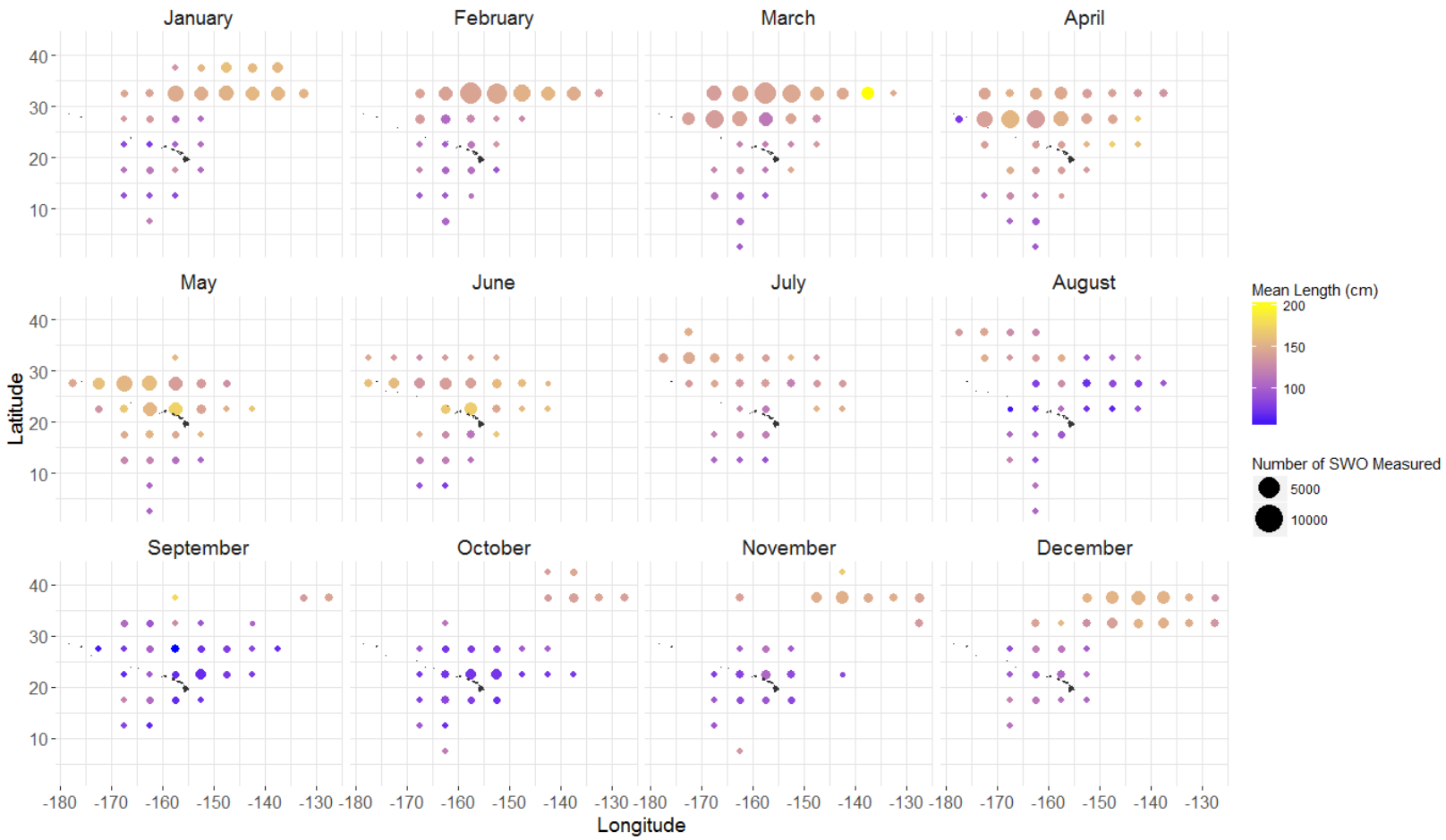

Figure 6. Monthly mean length of swordfish caught in both the deep and shallow-set sectors in 5° × 5° squares plotted over the Hawaiian Archipelago. Size of circles indicate number of swordfish measured, color indicates mean length.

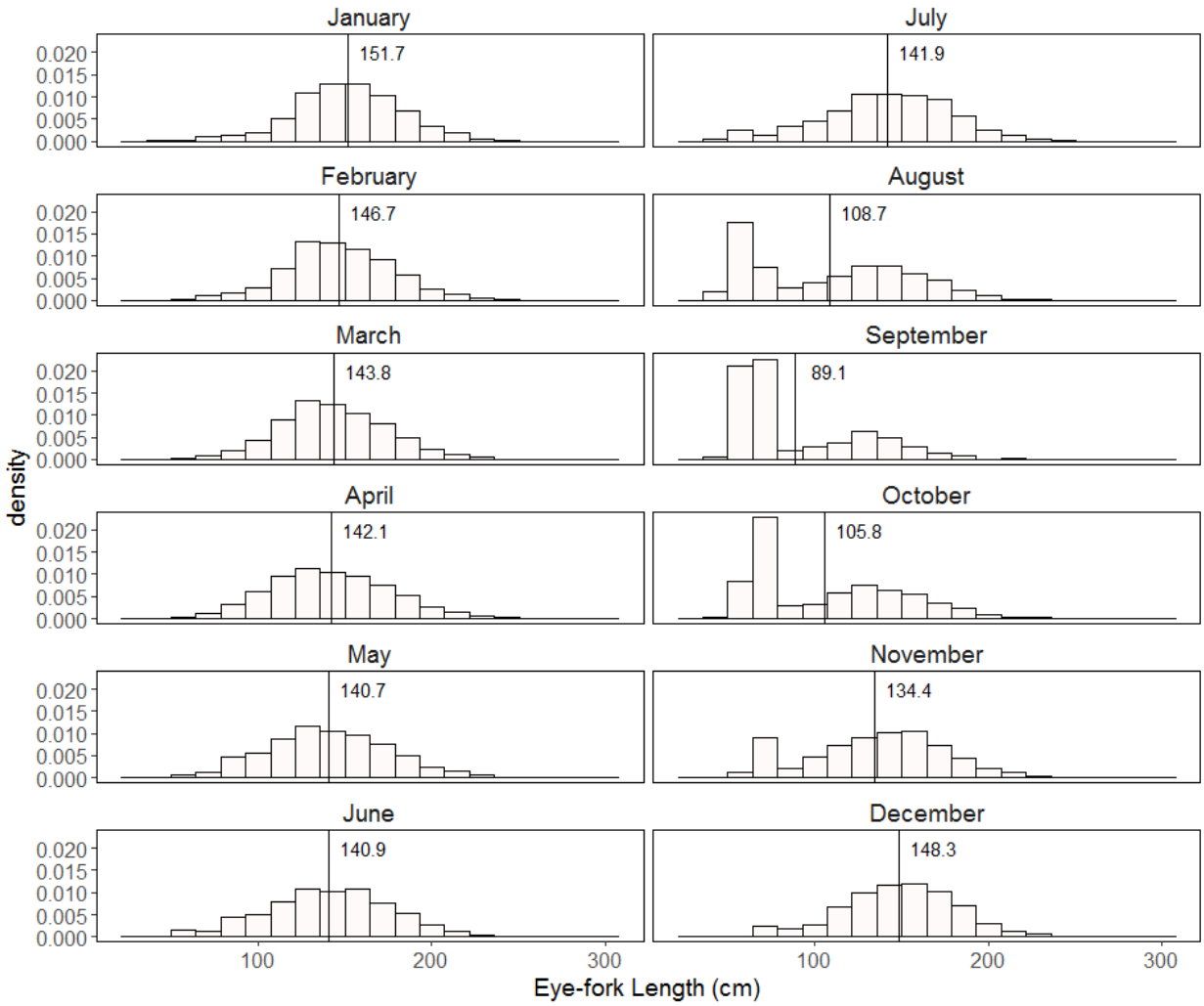

Figure 7. Histogram of swordfish length by month for both the deep- and shallow-set sectors. Vertical line indicates median length.

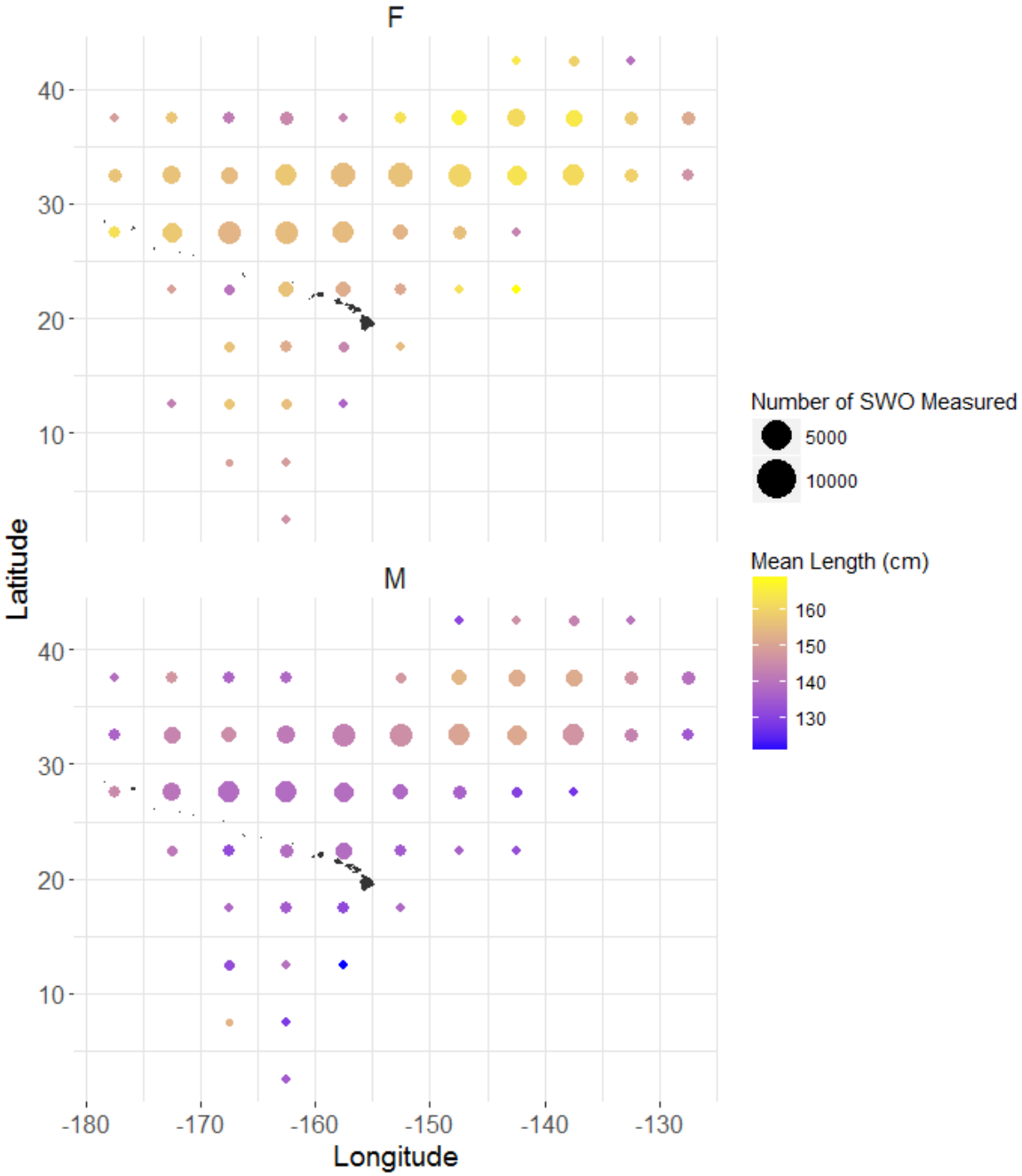

Figure 8. Mean length of female (top panel) and male (bottom panel) swordfish in 5° × 5° squares plotted over the Hawaiian Archipelago.

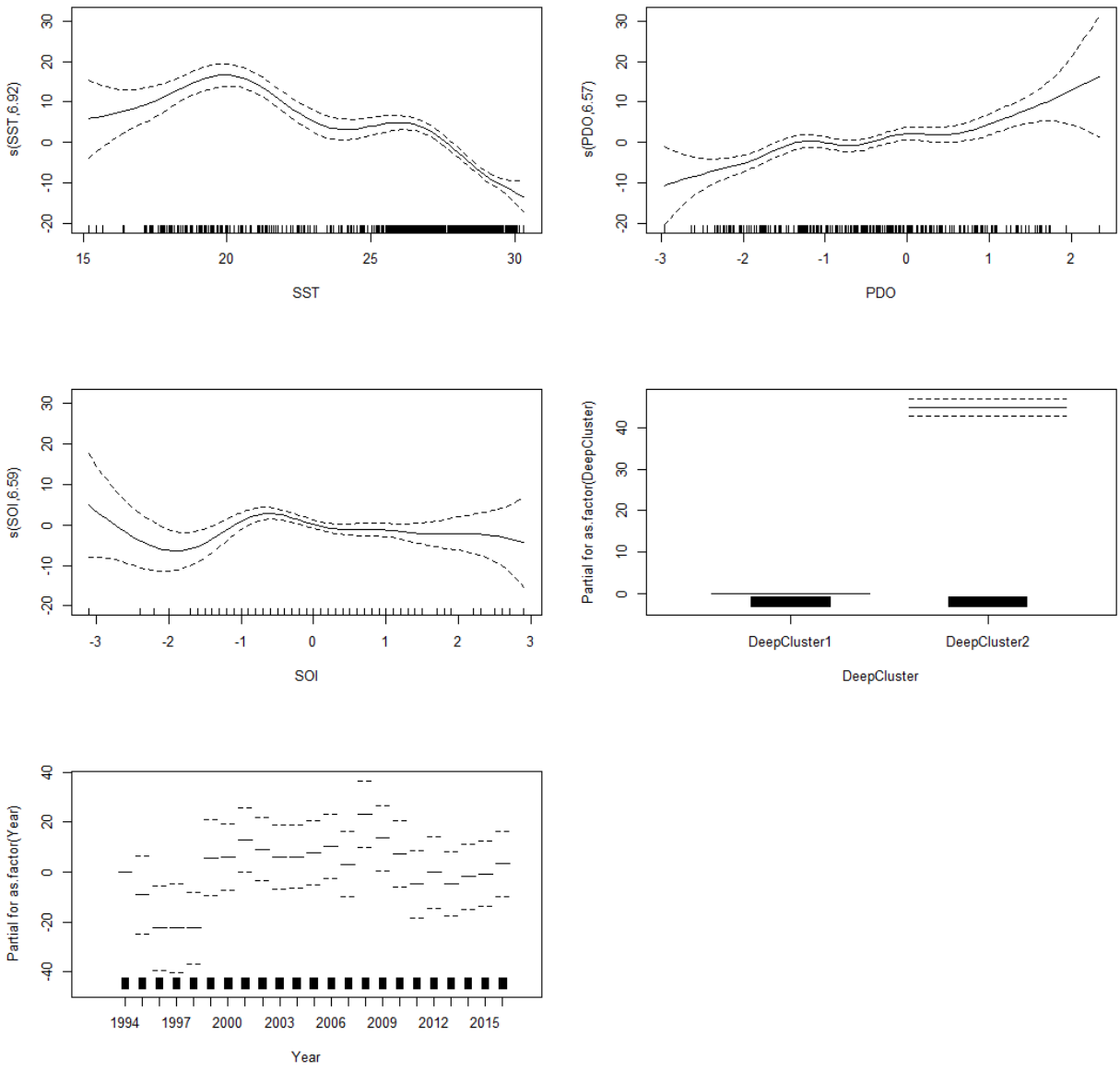

Figure 9. Model estimated partial effect (solid line) and ± 2 standard errors (dashed line) of sea surface temperature (top left), the Pacific Decadal Oscillation Index (top right), the Southern Oscillation Index (center left), the cluster (center right) and year (bottom left) for model D1.

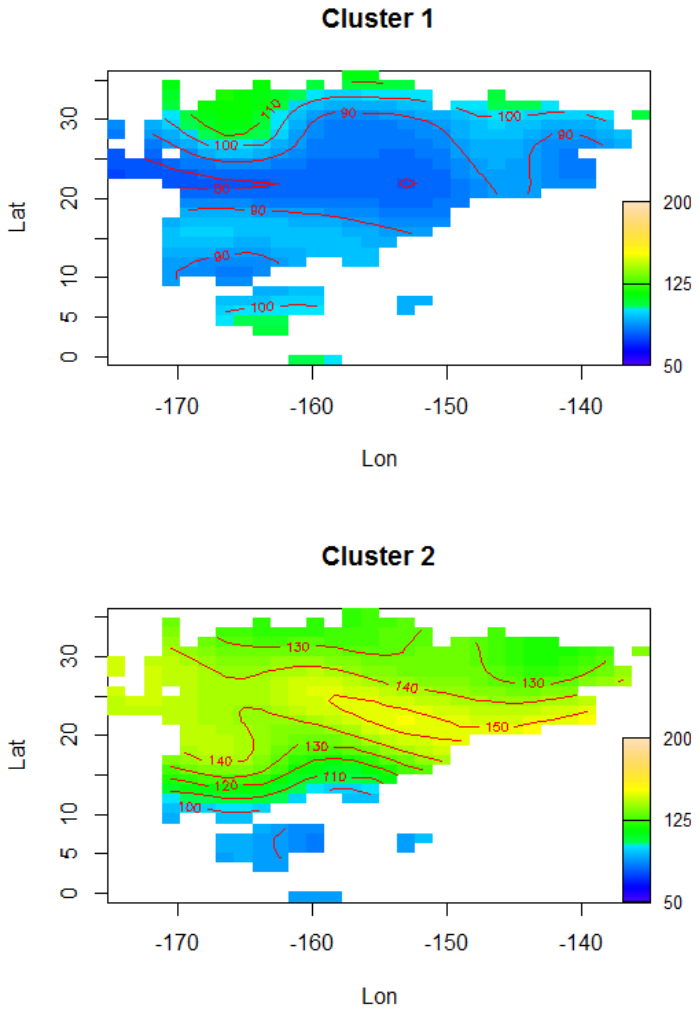

Figure 10. Predicted eye-fork lengths (in cm) of swordfish at 1° × 1° grids at the median value for each of the other variables included by cluster in model D1. Cluster 1 includes August–March. Cluster 2 includes April–July. Locations where there were measurements from less than three vessels were excluded for confidentiality.

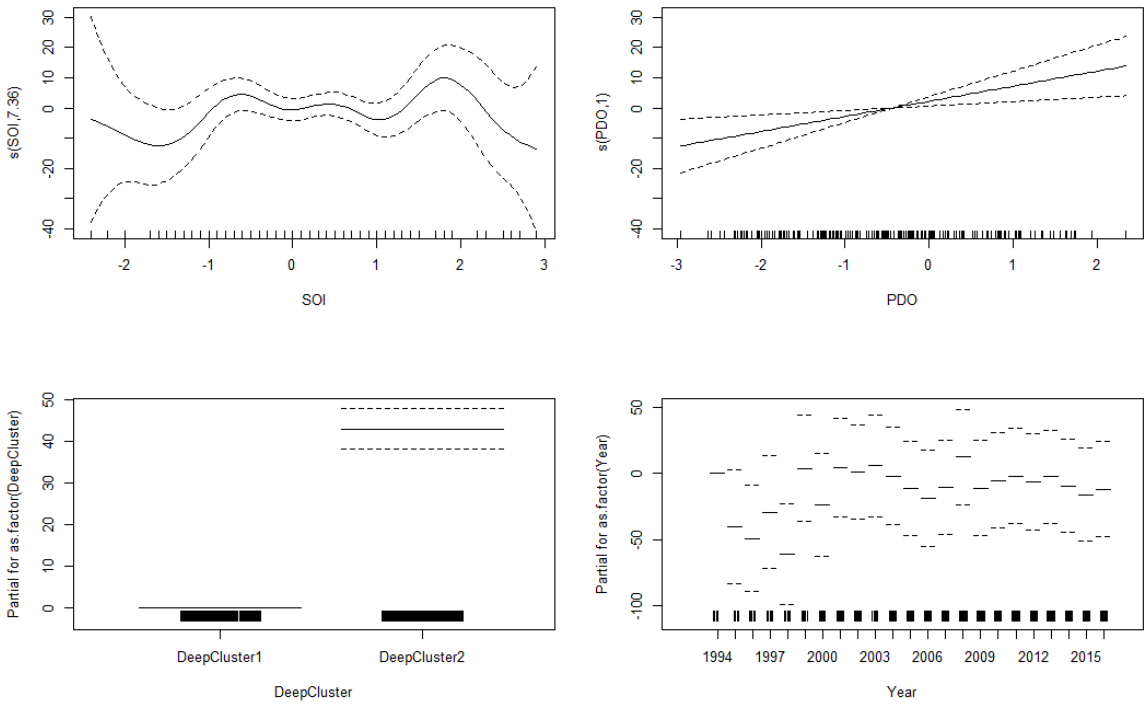

Figure 11. Model estimated partial effect (solid line) and ± 2 standard errors (dashed line) of the Southern Oscillation Index (top left), the Pacific Decadal Oscillation Index (top right), the cluster (bottom left) and year (bottom right) for the D2.

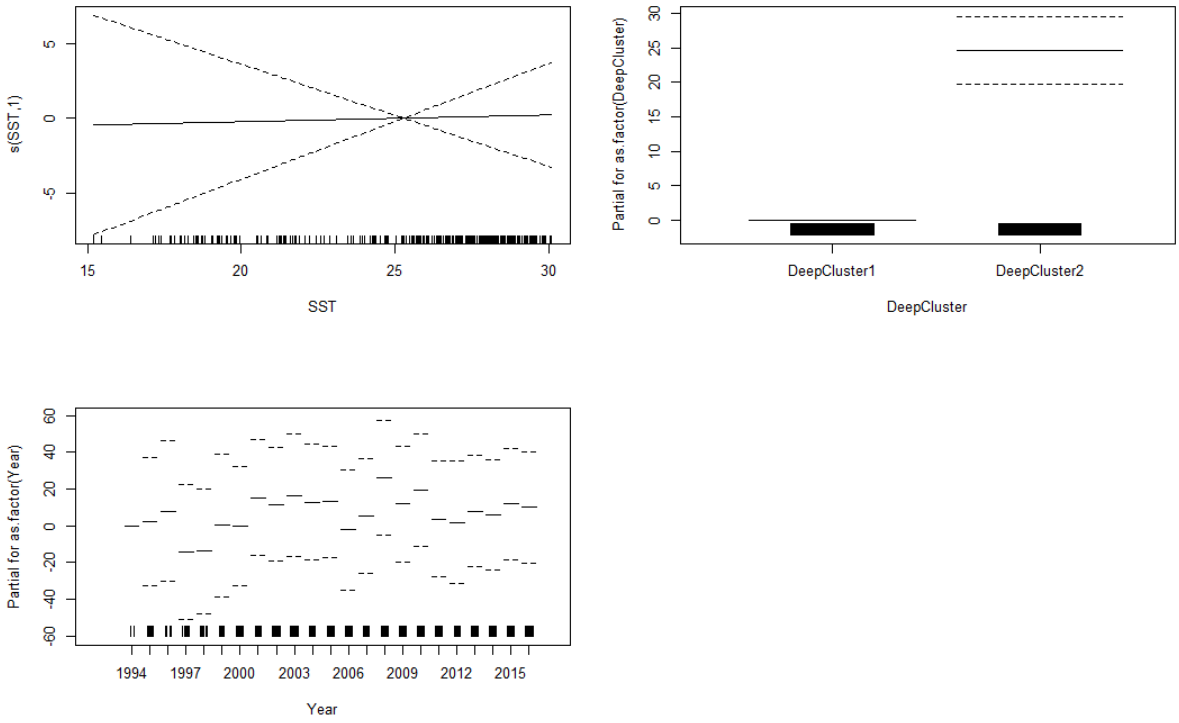

Figure 12. Model estimated partial effect (solid line) and ± 2 standard errors (dashed line) of sea surface temperature (top left), the cluster (top right) and year (bottom left) for the D3.

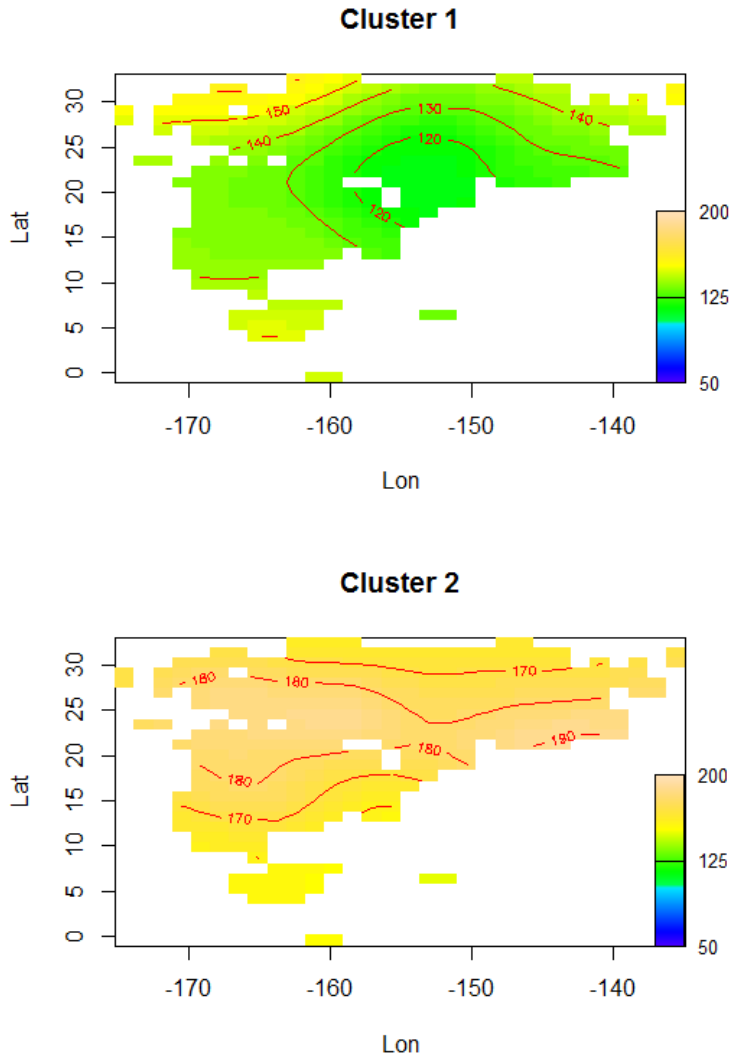

Figure 13. Predicted eye-fork lengths (in cm) of swordfish at 1° × 1° grids at the median value for each of the other variables included by cluster in model D2. Cluster 1 includes August–March. Cluster 2 includes April–July. Locations where there were measurements from less than three vessels were excluded for confidentiality.

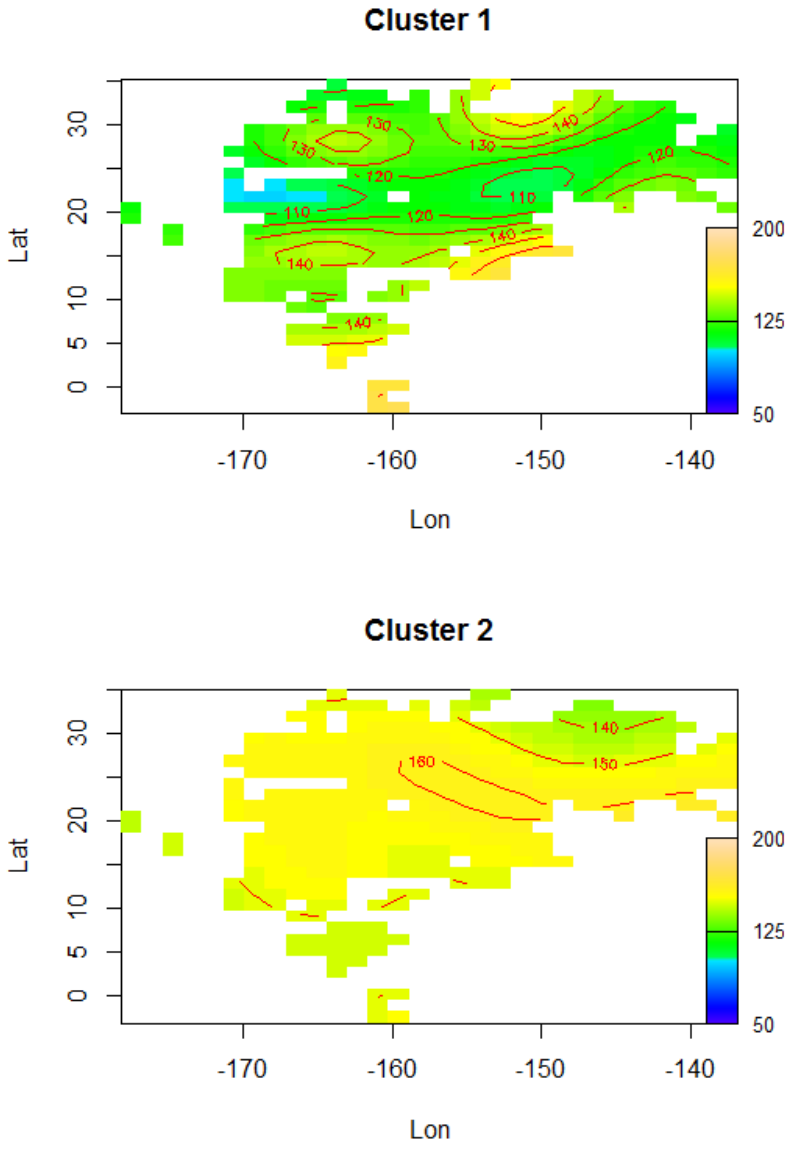

Figure 14. Predicted eye-fork lengths (in cm) of swordfish at 1° × 1° grids at the median value for each of the other variables included by cluster in model D3. Cluster 1 includes August–March. Cluster 2 includes April–July. Locations where there were measurements from less than three vessels were excluded for confidentiality.

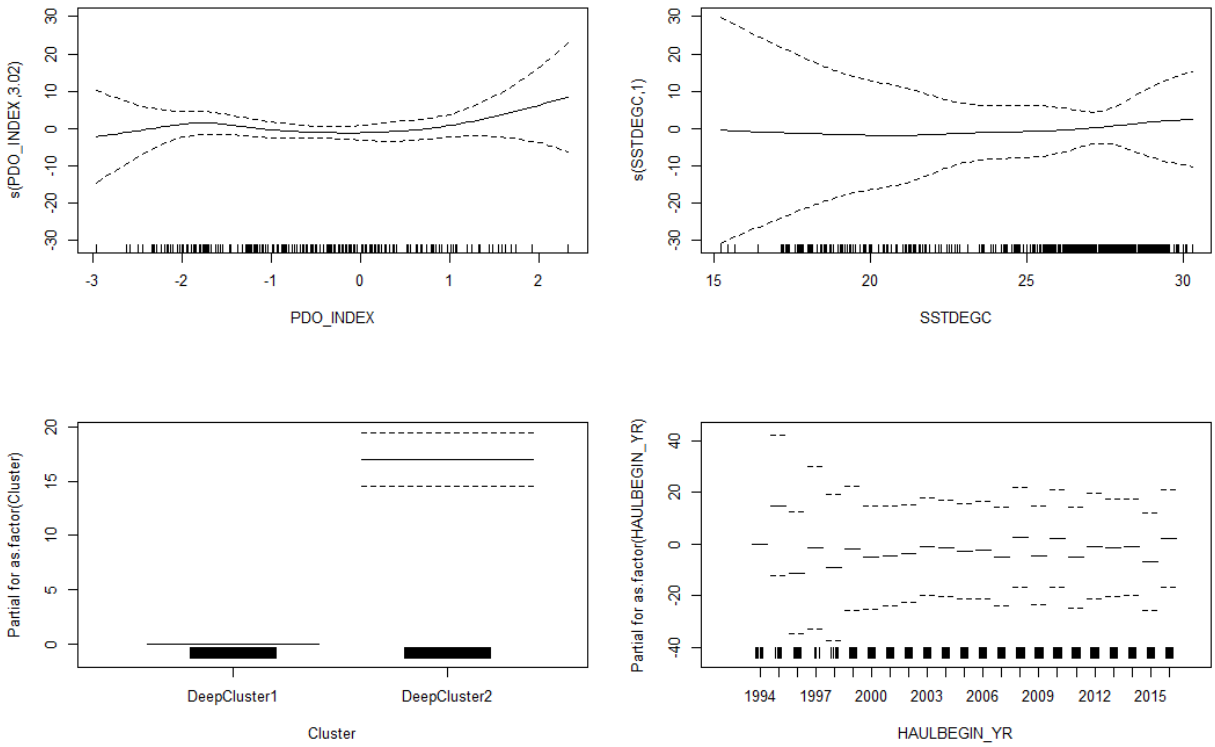

Figure 15. Model estimated partial effect (solid line) and ± 2 standard errors (dashed line) of the Pacific Decadal Oscillation Index (top left), sea surface temperature (top right), the cluster (bottom left) and year (bottom right) for model D4.

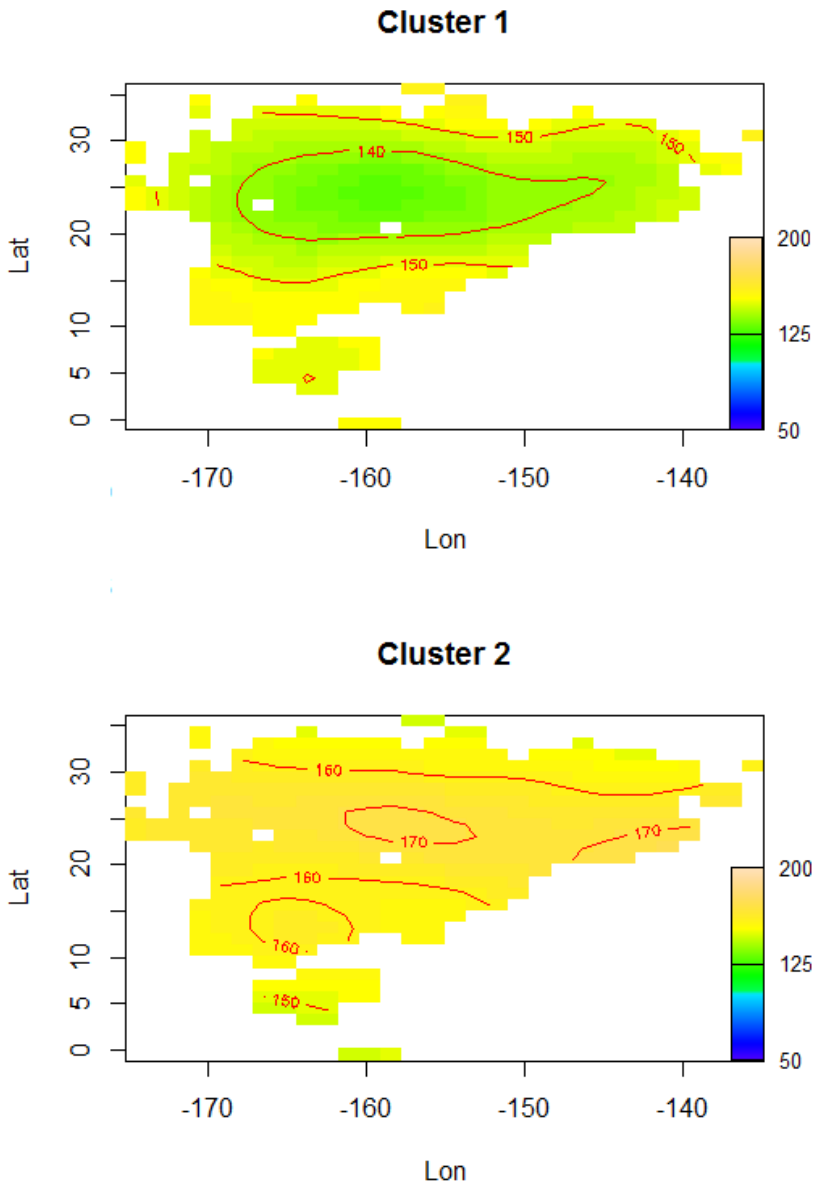

Figure 16. Predicted eye-fork lengths (in cm) of swordfish at 1° × 1° grids at the median value for each of the other variables included by cluster in model D4. Cluster 1 includes August–March. Cluster 2 includes April–July. Locations where there were measurements from less than three vessels were excluded for confidentiality.

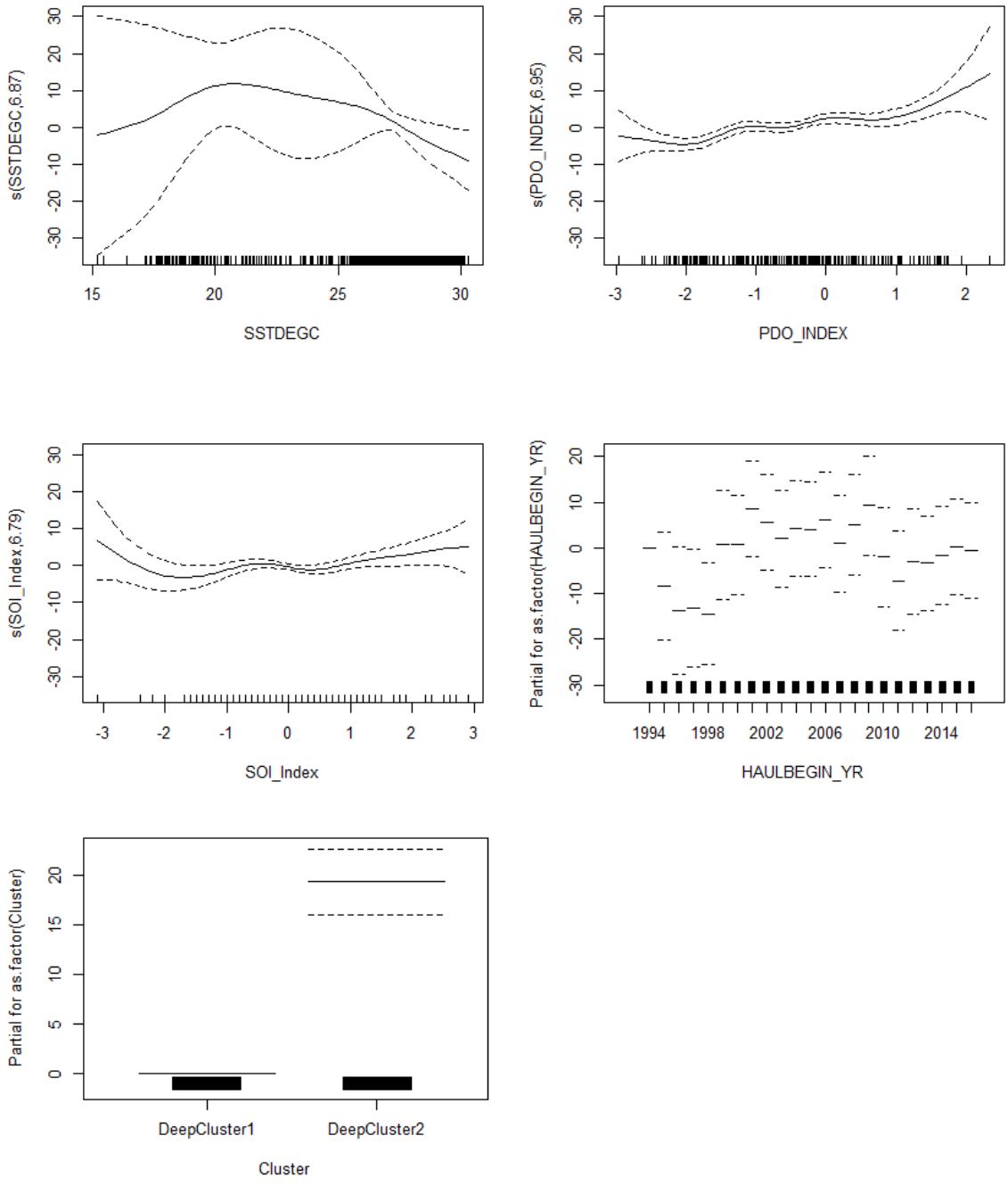

Figure 17. Model estimated partial effect (solid line) and ± 2 standard errors (dashed line) of sea surface temperature (top left), the Pacific Decadal Oscillation Index (top right), the Southern Oscillation Index (center left), the year (center right), and cluster (bottom left) for model D5.

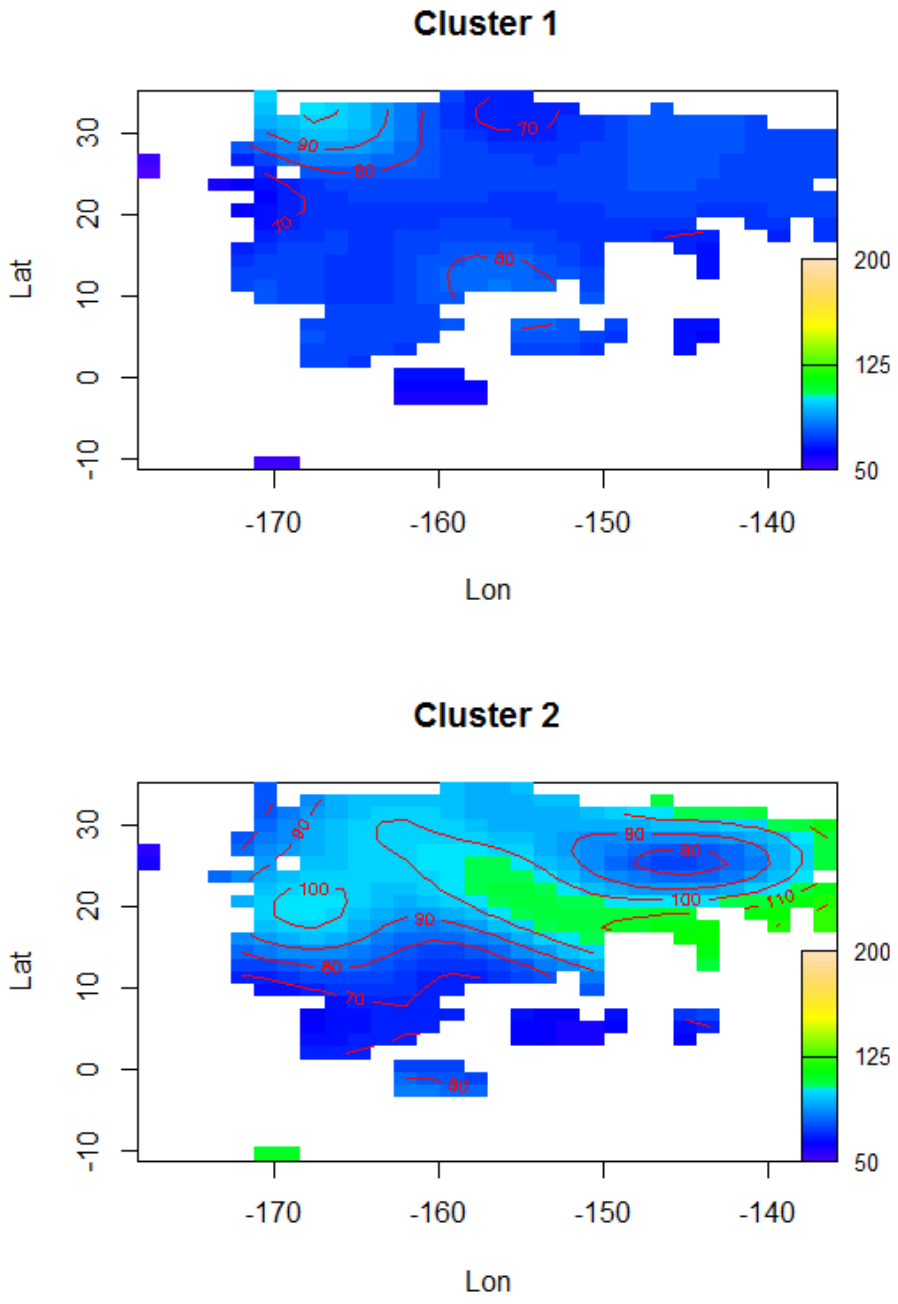

Figure 18. Predicted eye-fork lengths (in cm) of swordfish at 1° × 1° grids at the median value for each of the other variables included by cluster for model D5. Cluster one includes August–March. Cluster two includes April–July. Locations where there were measurements from less than three vessels were excluded for confidentiality.

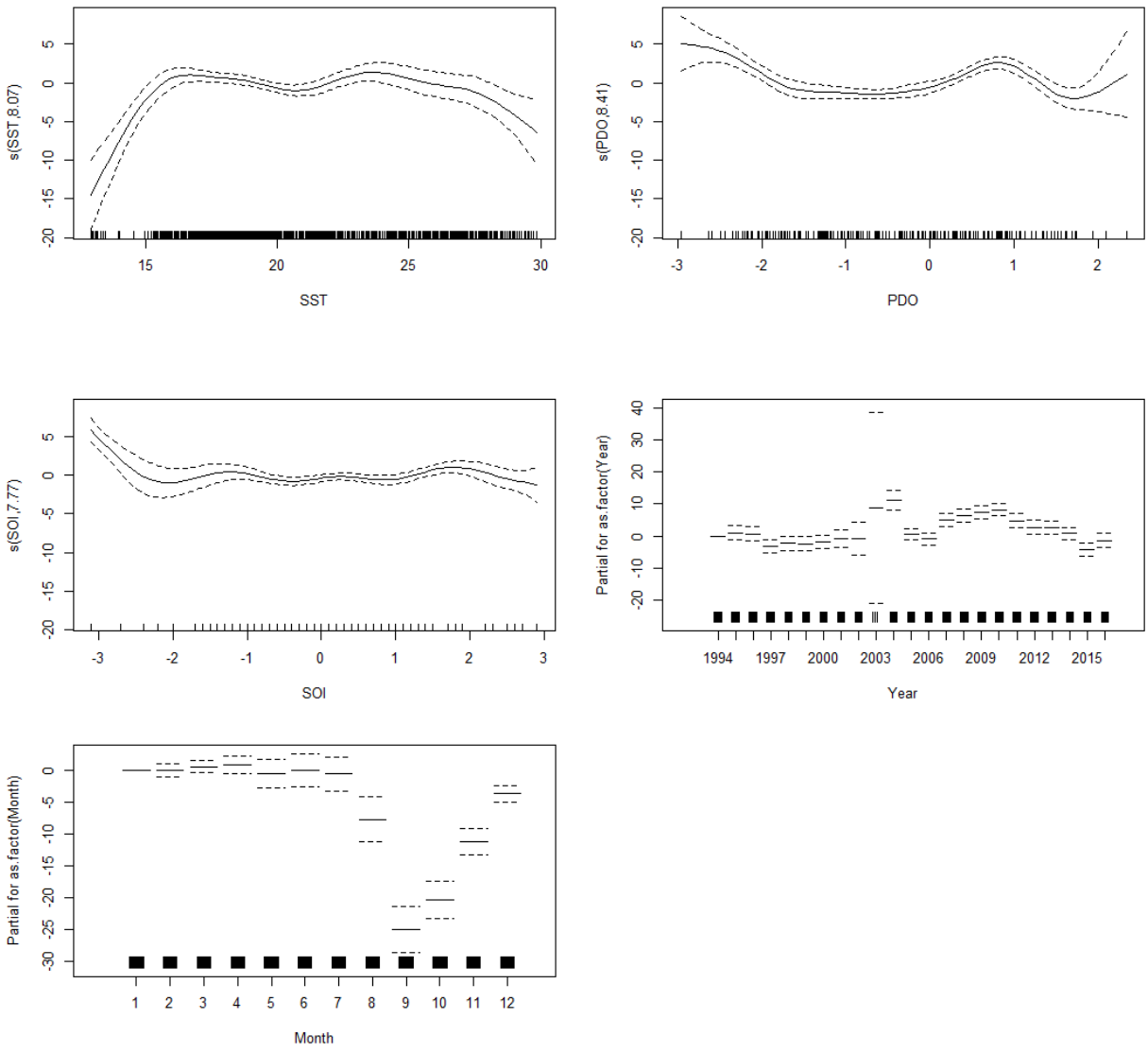

Figure 19. Model estimated partial effect (solid line) and ± 2 standard errors (dashed line) of sea surface temperature (top left), the Pacific Decadal Oscillation Index (top right), the Southern Oscillation Index (center left), the year (center right), and month (bottom left) for model S1.

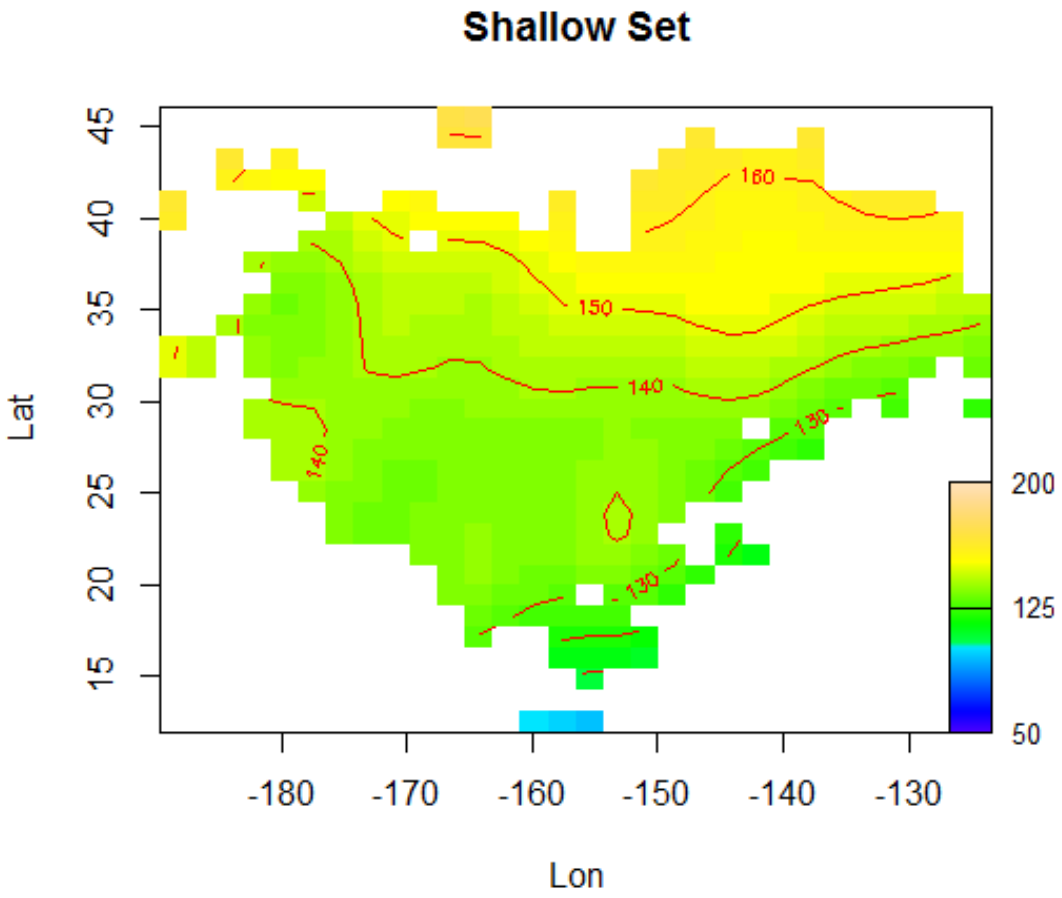

Figure 20. Predicted eye-fork lengths (in cm) of swordfish at 1° × 1° grids at the median value for each of the other variables included in model S1. Locations where there were measurements from less than three vessels were excluded for confidentiality.

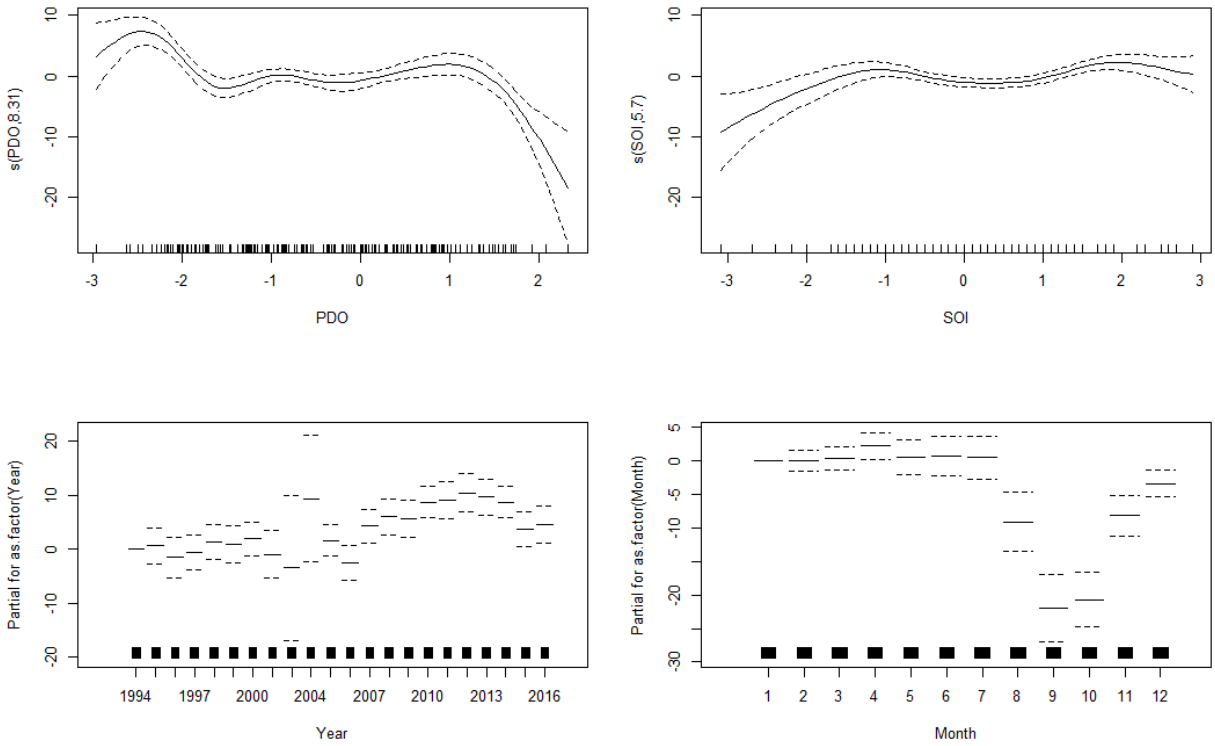

Figure 21. Model estimated partial effect (solid line) and ± 2 standard errors (dashed line) of the Pacific Decadal Oscillation Index (top left), the Southern Oscillation Index (top right), the year (bottom left), and month (bottom right) for model S2.

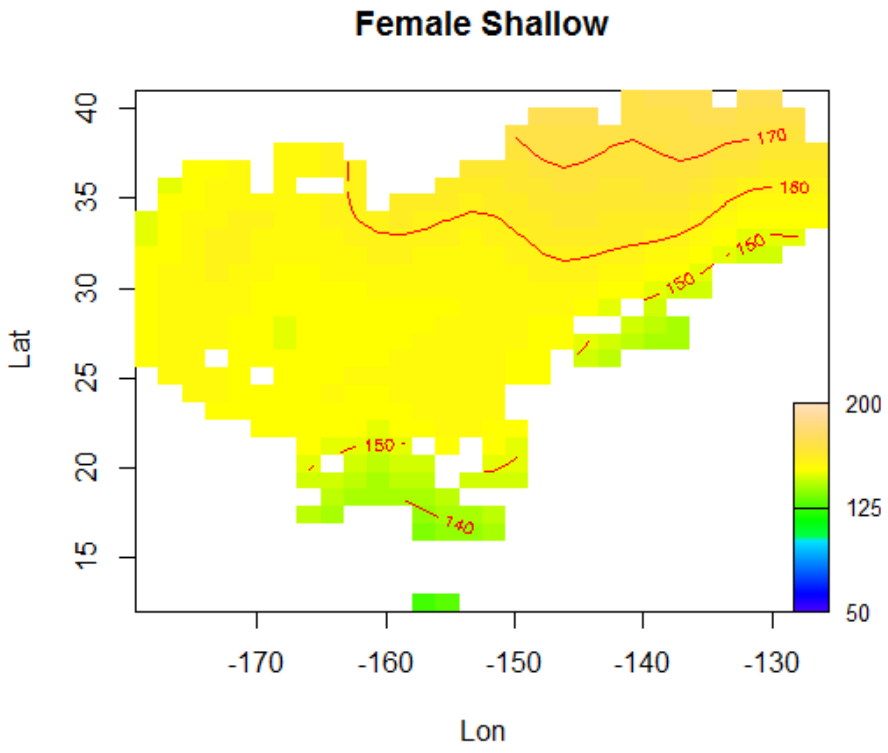

Figure 22. Predicted eye-fork lengths (in cm) of swordfish at 1° × 1° grids at the median value for each of the other variables included in model S2. Locations where there were measurements from less than three vessels were excluded for confidentiality.

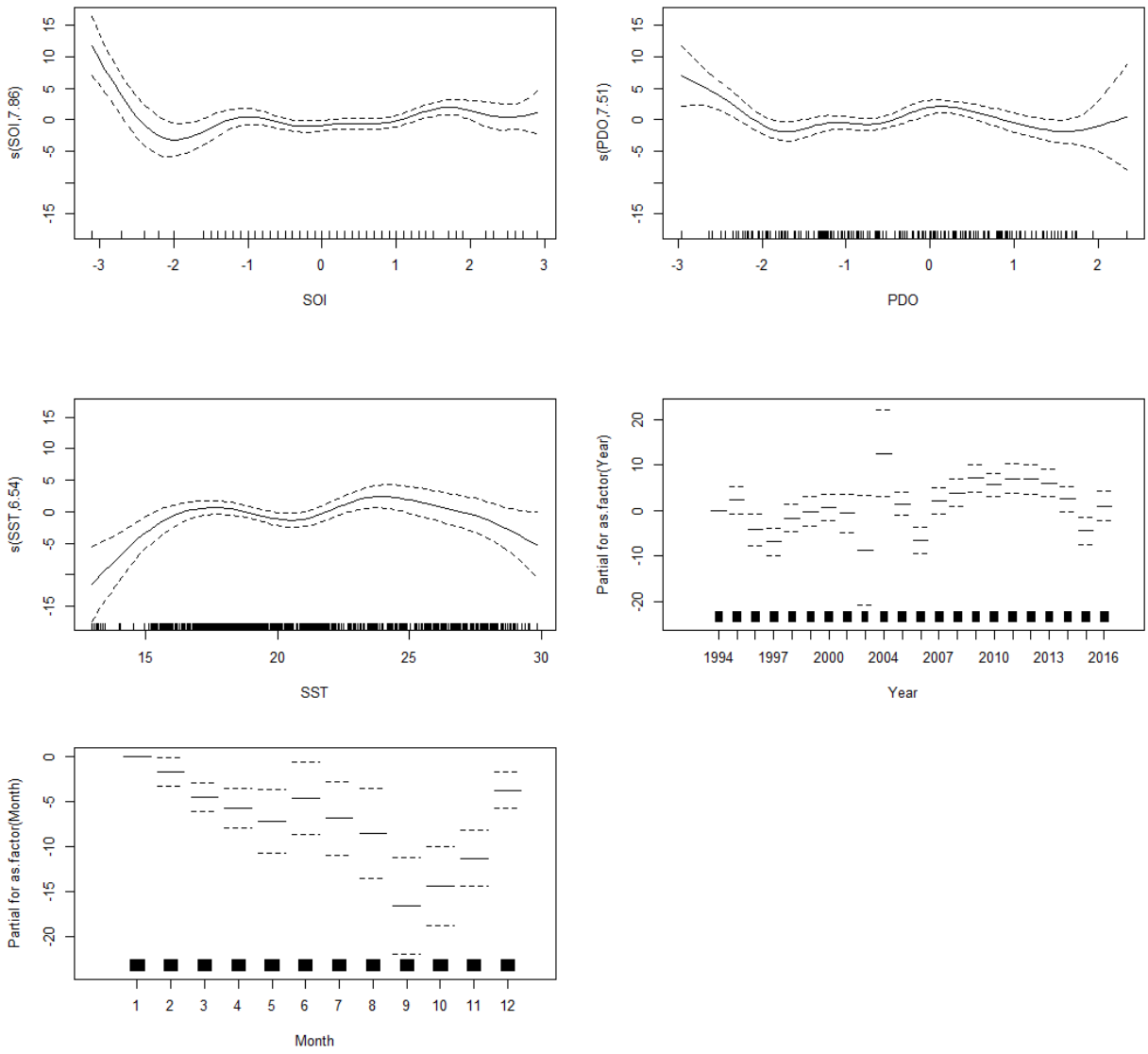

Figure 23. Model estimated partial effect (solid line) and ± 2 standard errors (dashed line) of the Southern Oscillation Index (top left), the Pacific Decadal Oscillation Index (top right), sea surface temperature (center left), the year (center right), and month (bottom left) for model S3.

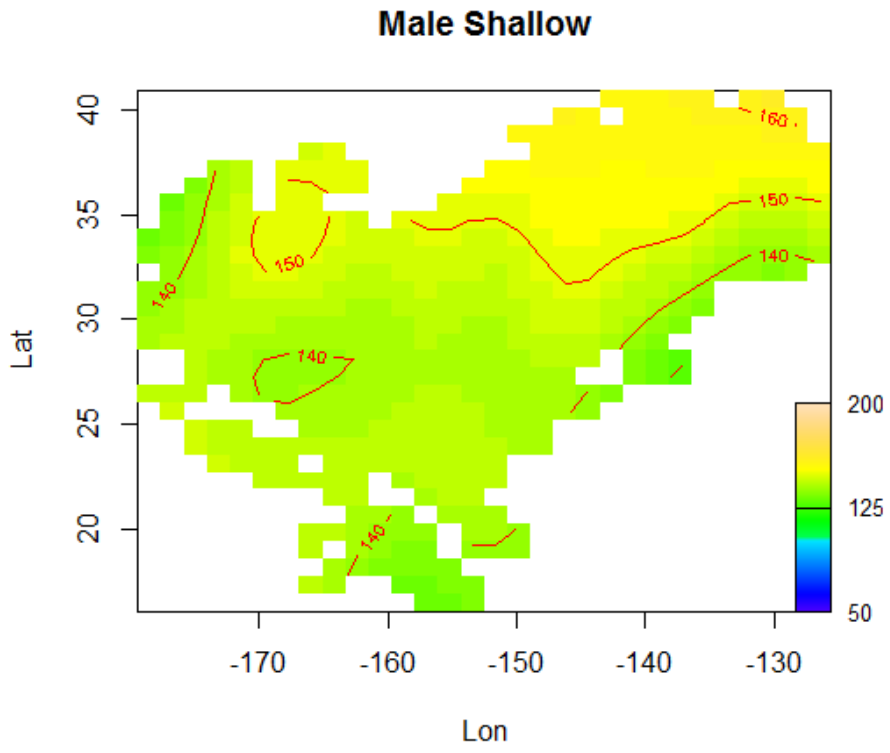

Figure 24. Predicted eye-fork lengths (in cm) of swordfish at 1° × 1° grids at the median value for each of the other variables included in model S3. Locations where there were measurements from less than three vessels were excluded for confidentiality.

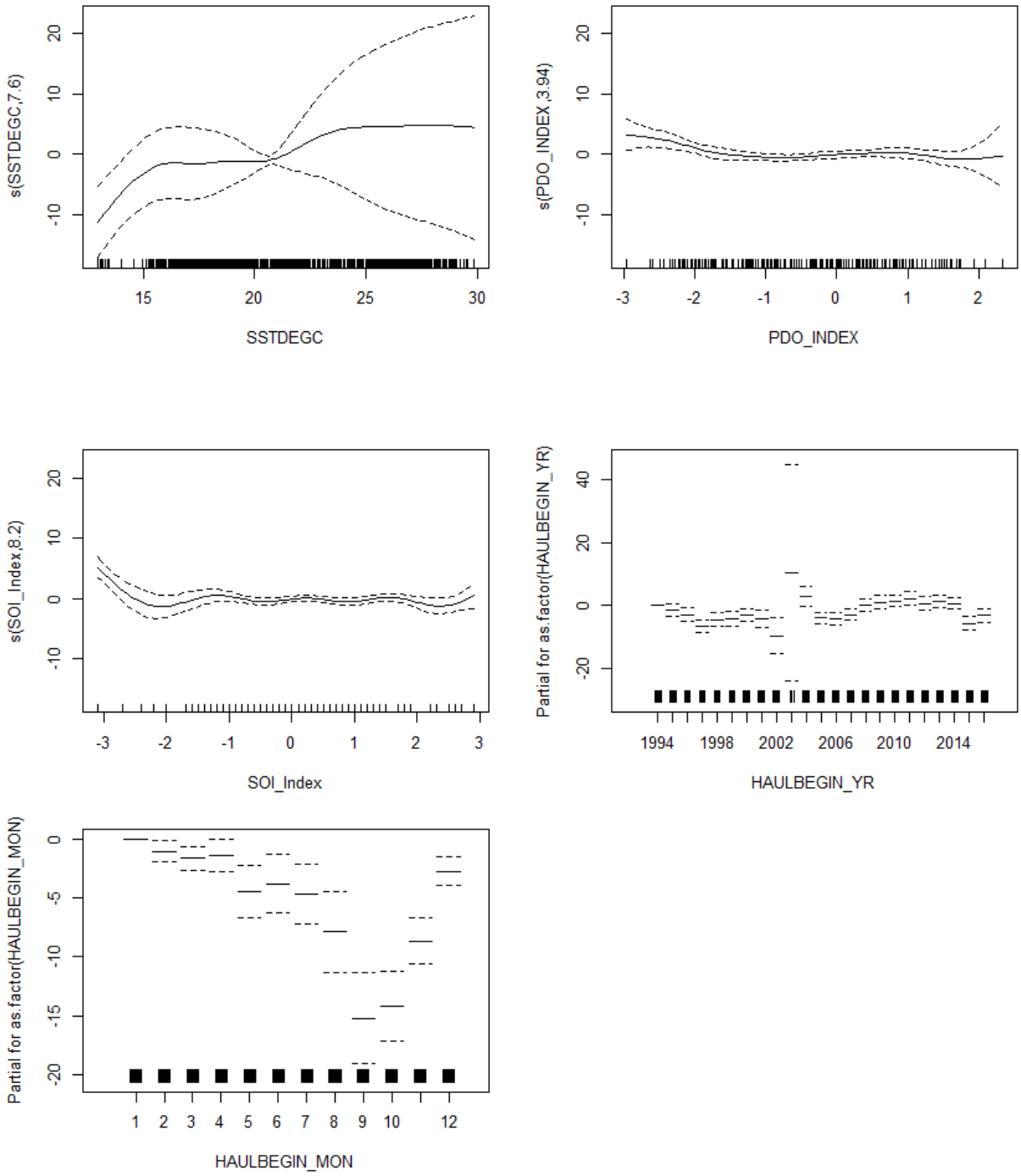

Figure 25. Model estimated partial effect (solid line) and ± 2 standard errors (dashed line) of sea surface temperature (top left), the Pacific Decadal Oscillation Index (top right), the Southern Oscillation Index (center left), the year (center right), and month (bottom left) for model S4.

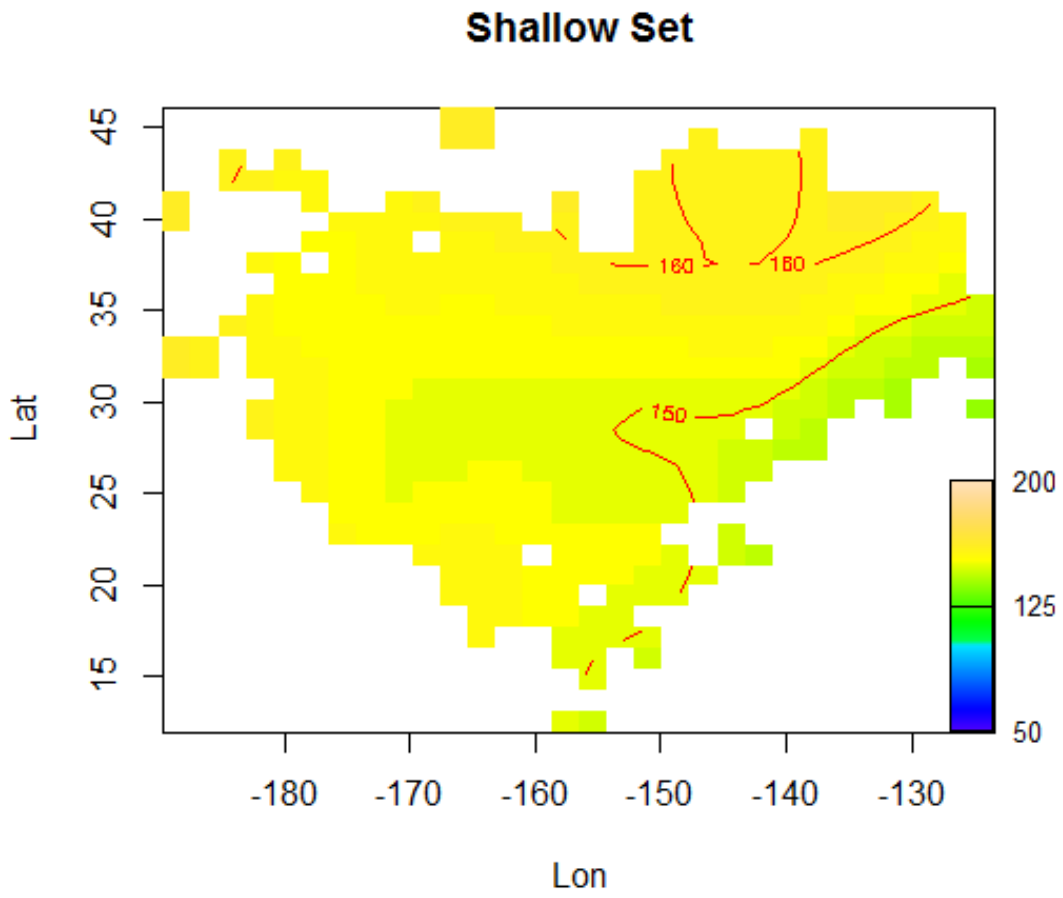

Figure 26. Predicted eye-fork lengths (in cm) of swordfish at 1° × 1° grids at the median value for each of the other variables included in model S4. Locations where there were measurements from less than three vessels were excluded for confidentiality.

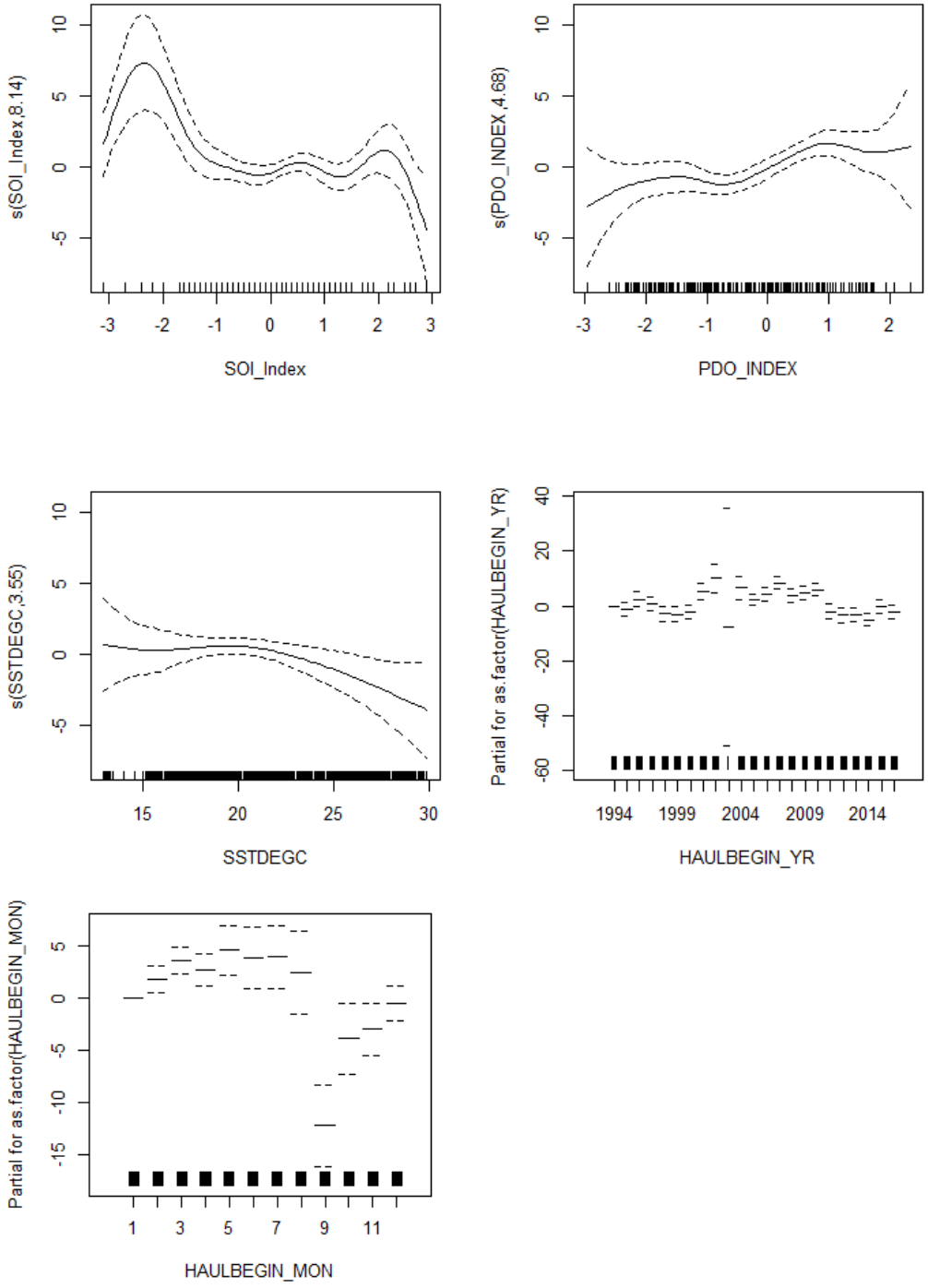

Figure 27. Model estimated partial effect (solid line) and ± 2 standard errors (dashed line) of the Southern Oscillation Index (top left), the Pacific Decadal Oscillation Index (top right), sea surface temperature (center left), the year (center right), and month (bottom left) for model S5.

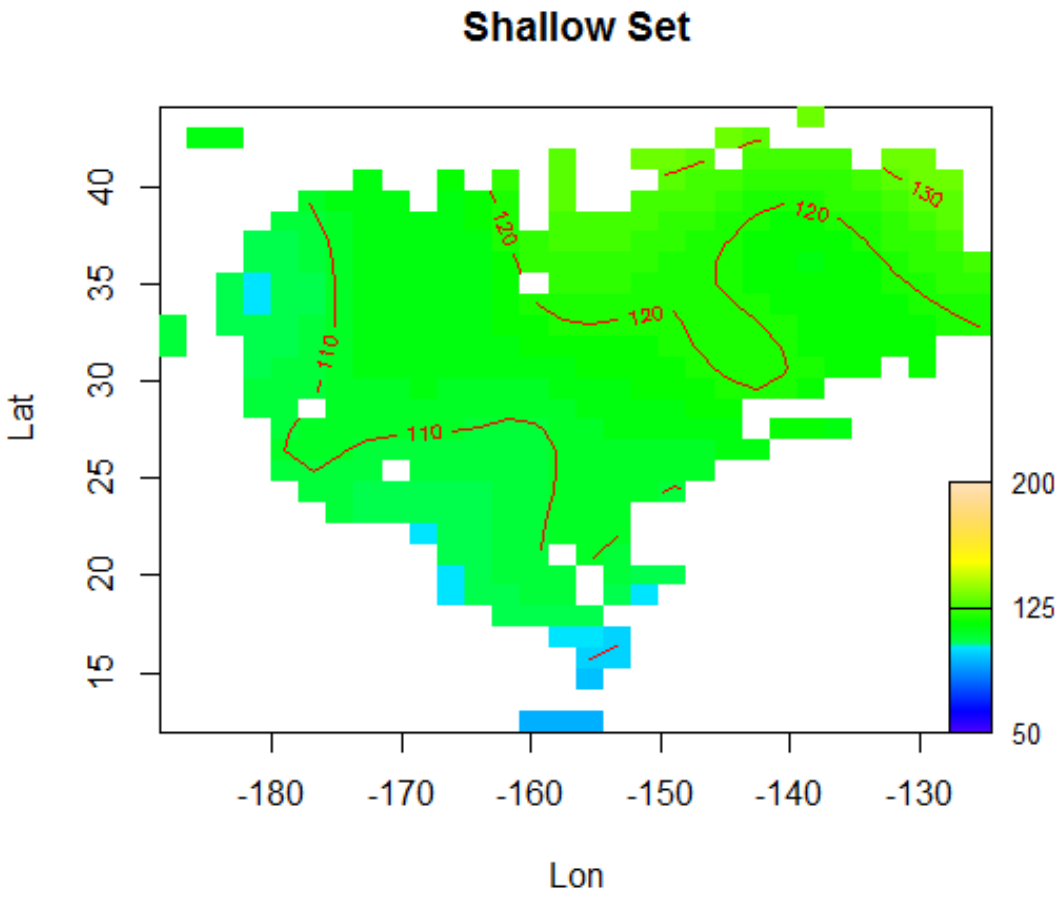

Figure 28. Predicted eye-fork lengths (in cm) of swordfish at 1° × 1° grids at the median value for each of the other variables included in model S5. Locations where there were measurements from less than three vessels were excluded for confidentiality.

Appendix 1

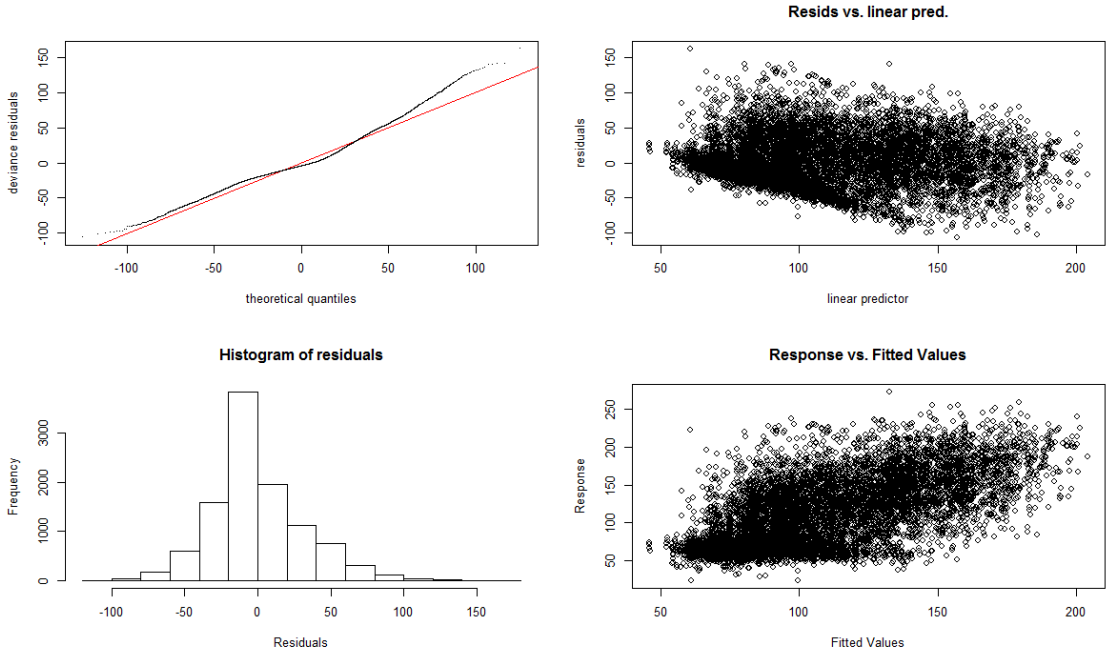

Figure A1. Diagnostic plot for model D1.

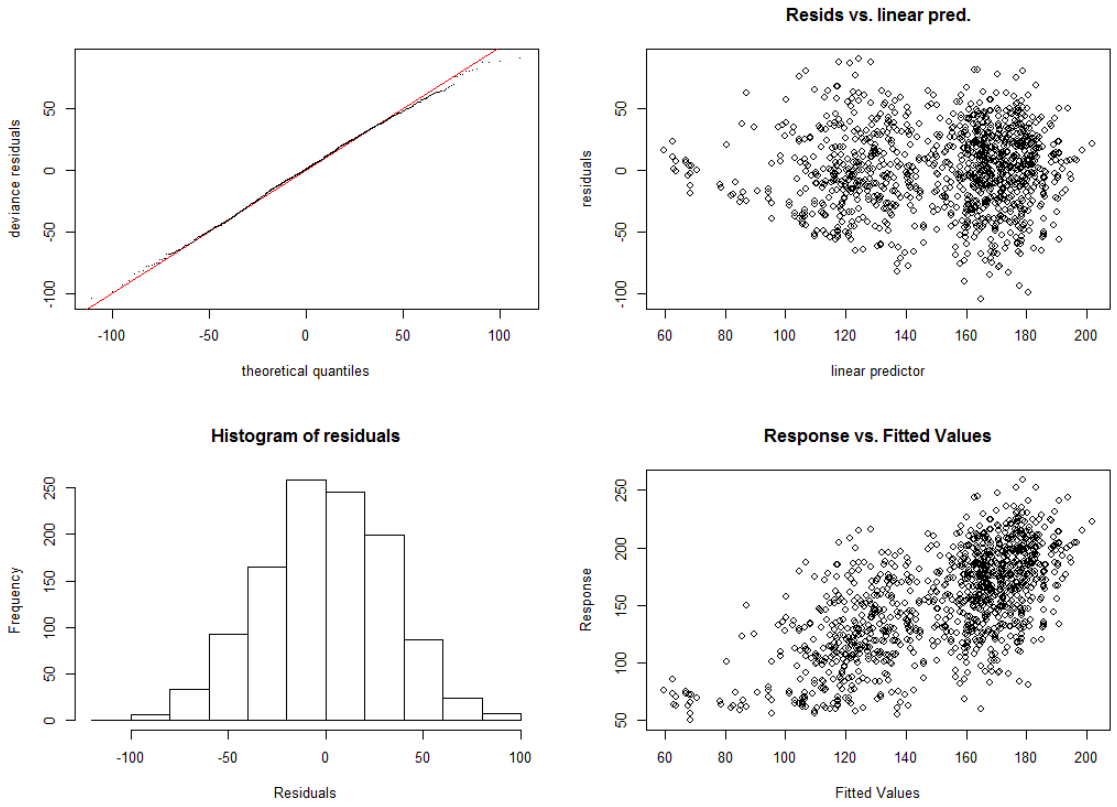

Figure A2. Diagnostic plot for the model D2.

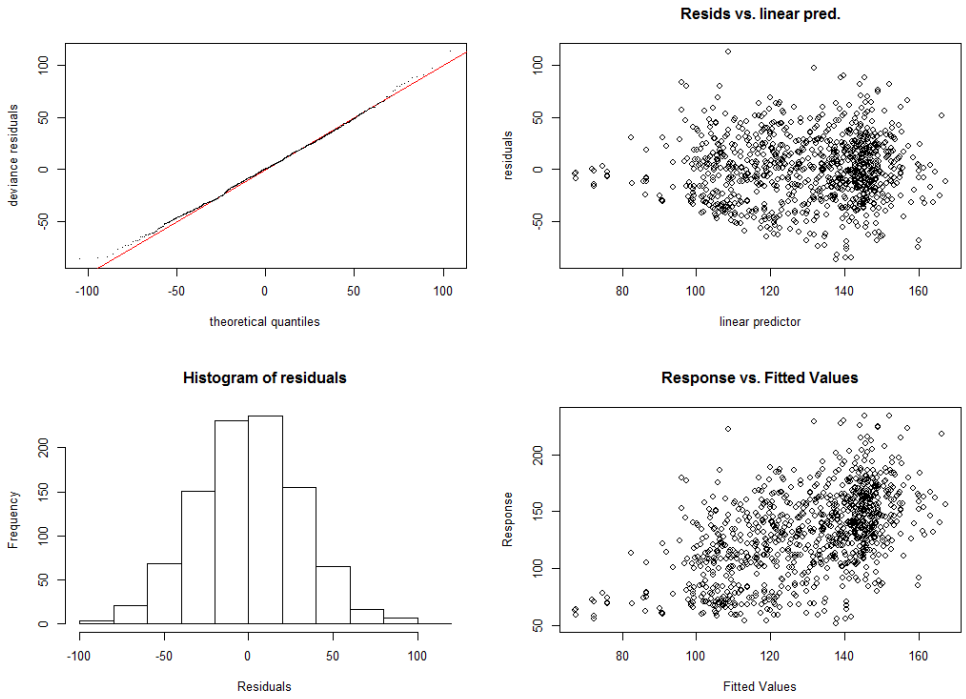

Figure A3. Diagnostic plot for model D3.

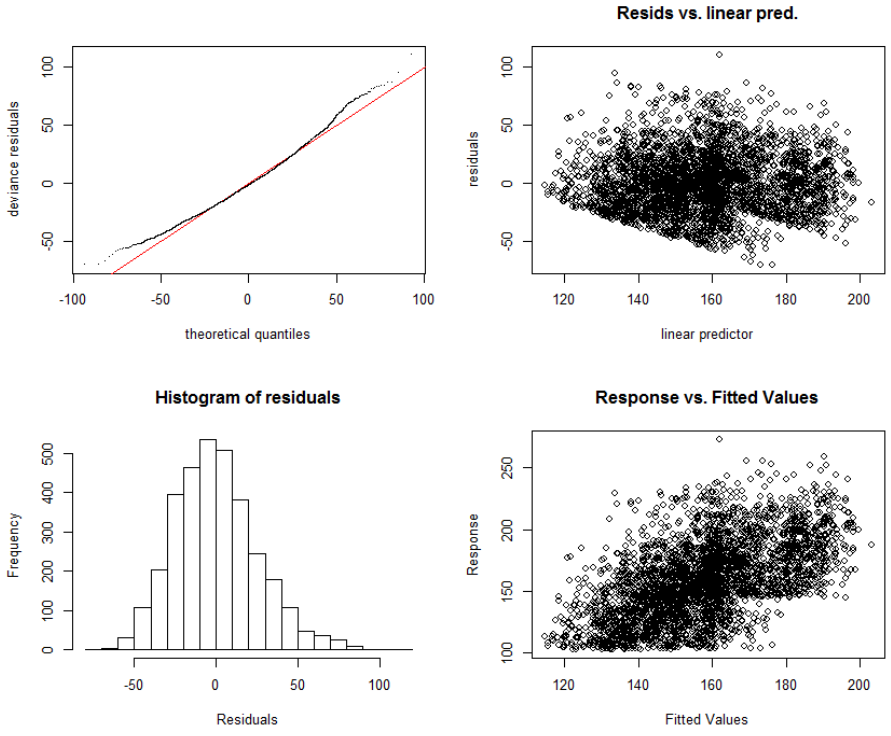

Figure A4. Diagnostic plot for one of the imputed D4 models.

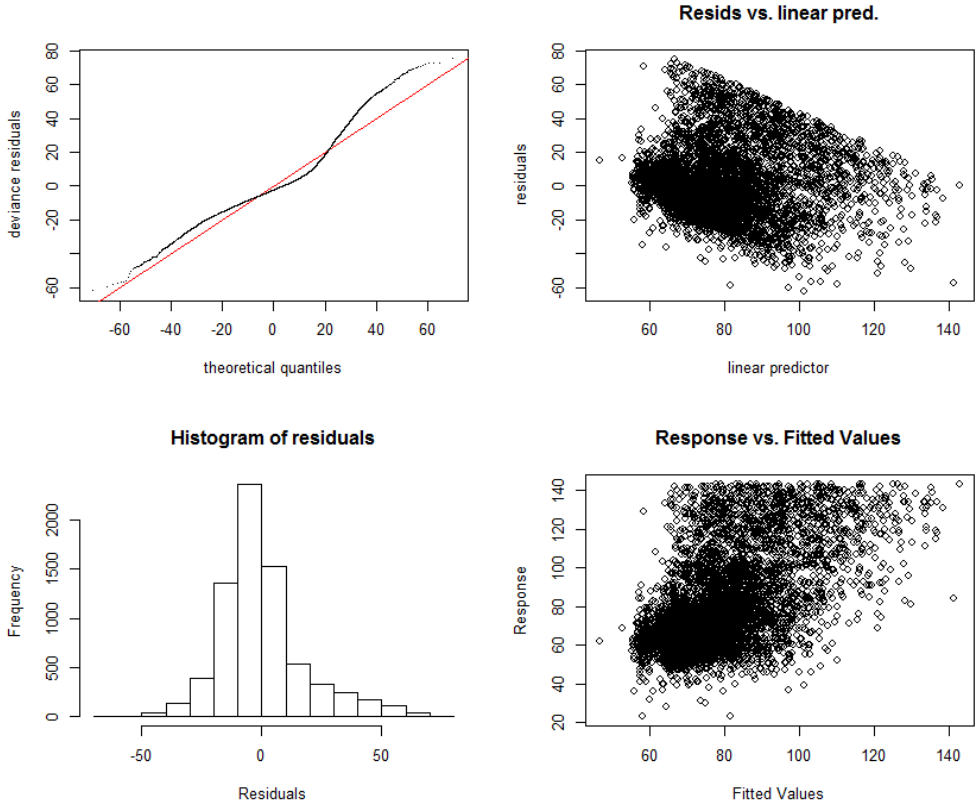

Figure A5. Diagnostic plot for one of the imputed D5 models.

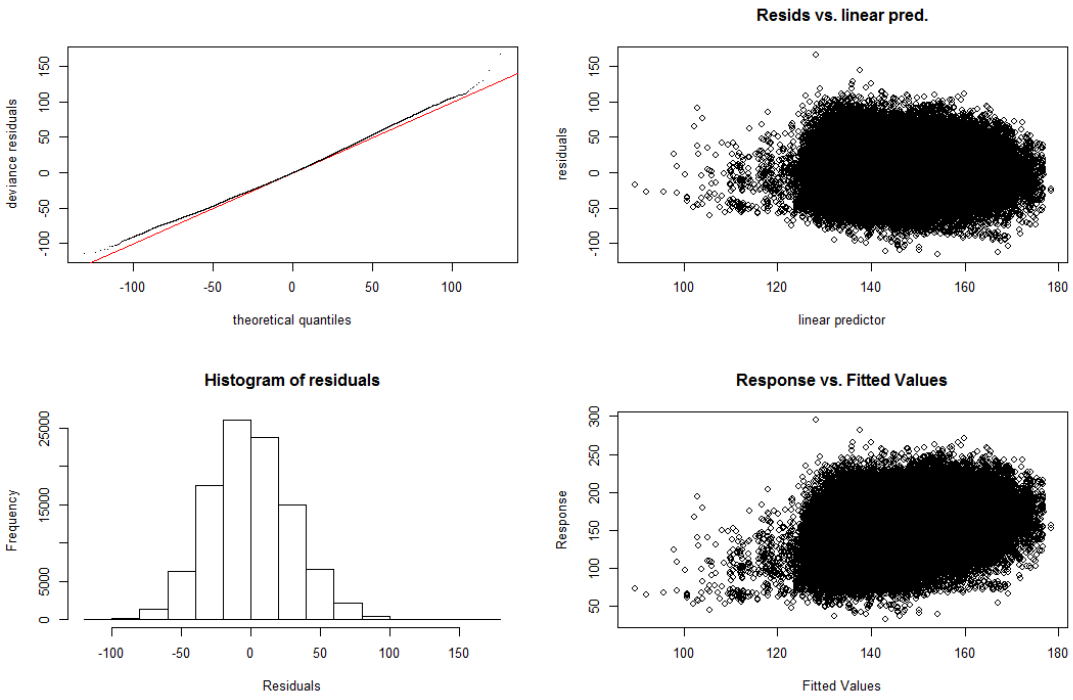

Figure A6. Diagnostic plot for model S1.

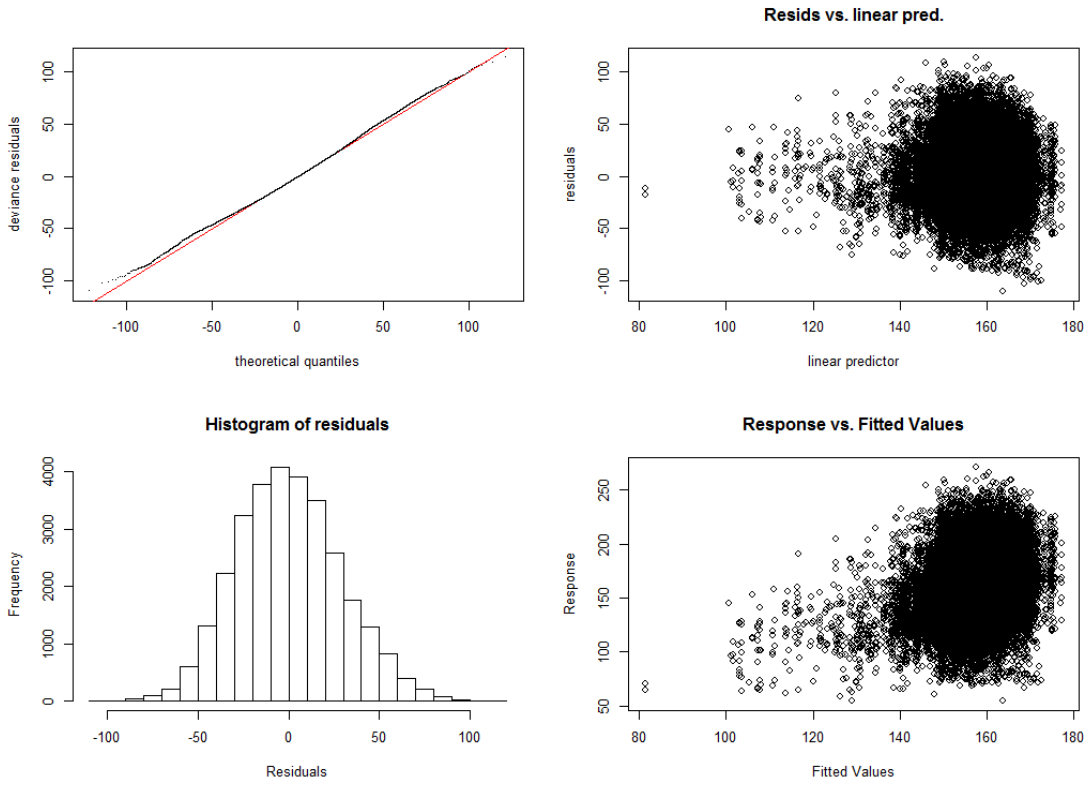

Figure A7. Diagnostic plot for model S2.

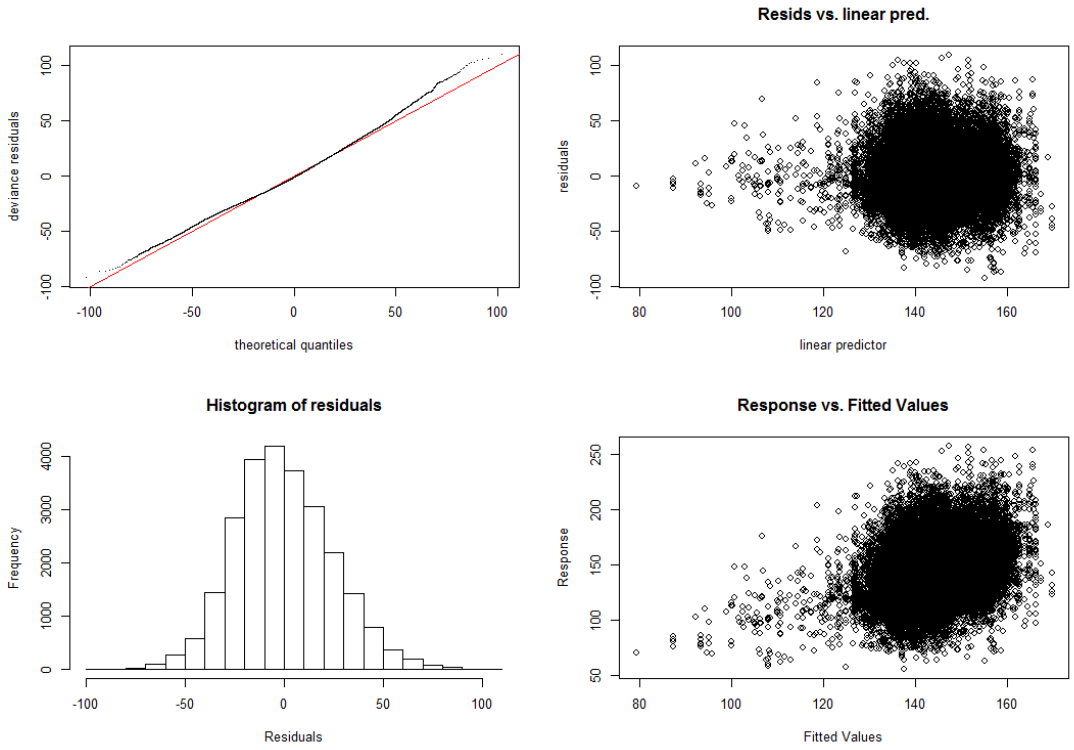

Figure A8. Diagnostic plot for model S3.

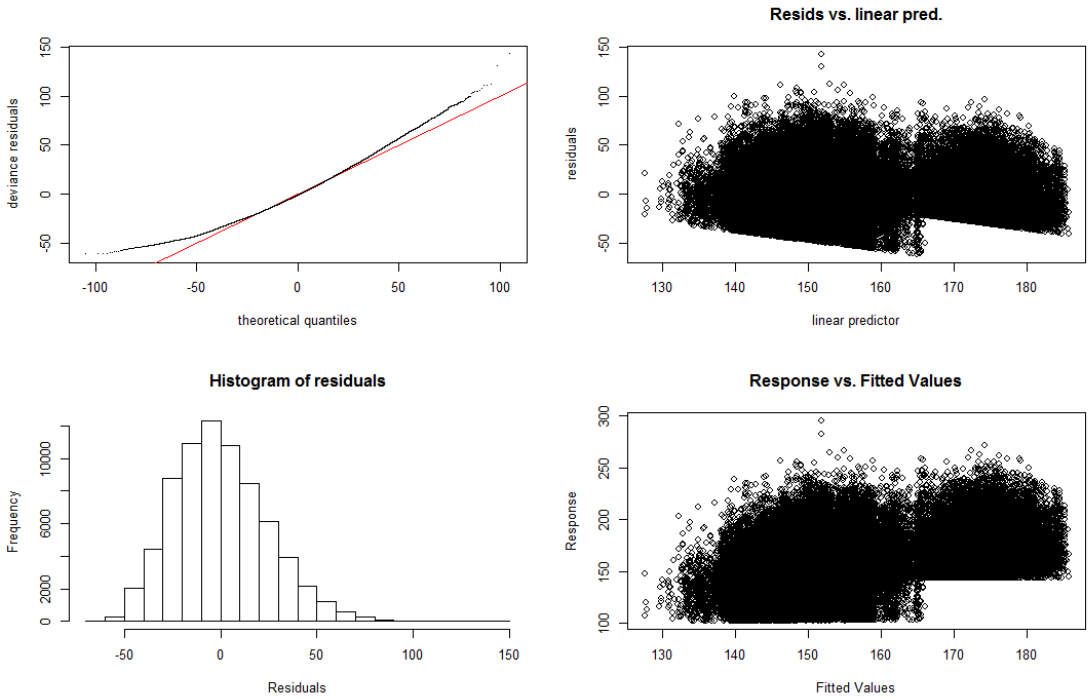

Figure A9. Diagnostic plot for one of the imputed S4 models.

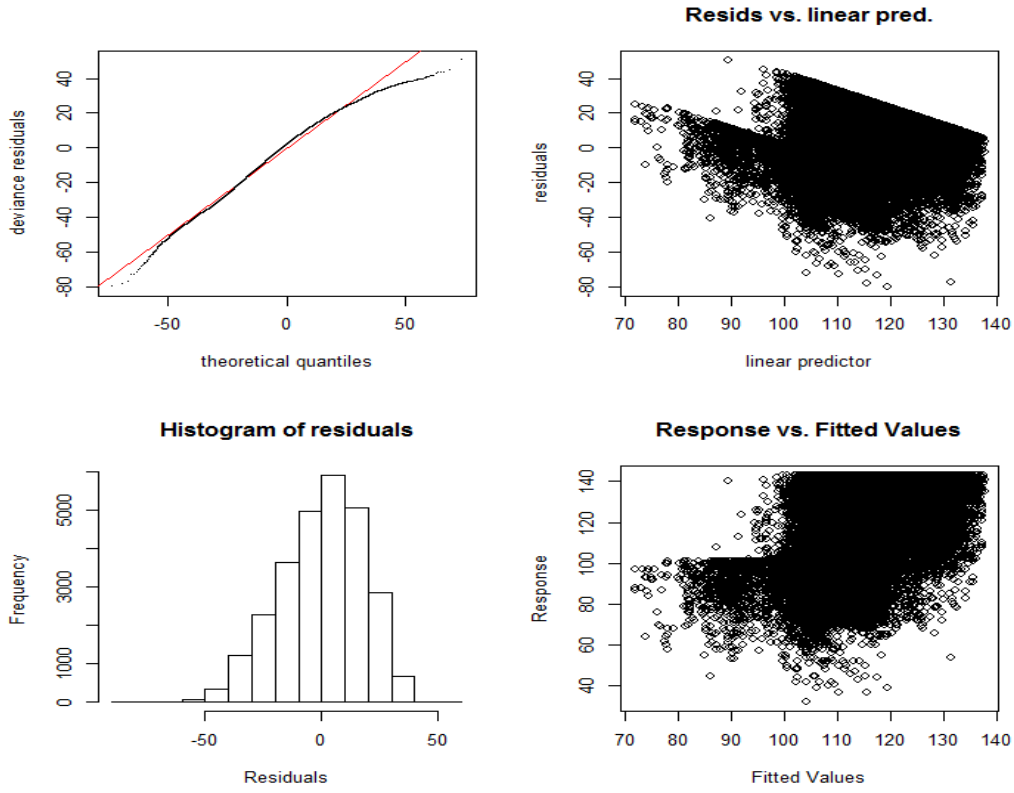

Figure A10. Diagnostic plot for one of the imputed S5 models.